International Applied Mechanics, Vol. 40, No. 9, 2004

MODELING THE THERMOMECHANICAL BEHAVIOR OF PHYSICALLY NONLINEAR MATERIALS UNDER MONOHARMONIC LOADING*

I. K. Senchenkov, Ya. A. Zhuk, and V. G. Karnaukhov UDC 539.376

We analyze approximate approaches to the modeling of the thermomechanical behavior of physically nonlinear materials under harmonic loading. The approaches are based on various harmonic-linearization schemes and the concept of complex moduli. Mechanical and mathematical features of various schemes are considered. Some modifications of the model are proposed to account for various aspects of material behavior under harmonic loading. The problems of vibration and dissipative heating of physically nonlinear bodies are formulated. The main thermomechanical characteristics are analyzed for some classes of problems.

Keywords: thermomechanical coupling, harmonic linearization, physically nonlinear material, monoharmonic loading, vibrations, dissipative heating

Introduction. Many structural elements and technological objects experience cyclic deformation during use or treatment [2, 3, 30–32, 61]. Loads are sometimes so high that the deformation process becomes nonlinear and mechanical elements may suffer low-cycle fatigue. Apart from purely mechanical fatigue failure, polymeric products may undergo thermal failure, i.e., softening or even melting due to vibrational heating, which is because of high hysteresis losses and low heat conductivity [32, 59, 60].

In the cases mentioned, modeling the thermomechanical behavior of nonlinearly dissipative materials is one of the major tasks to be accomplished in evaluating the durability or working characteristics of cyclically deformed bodies.

There are currently two approaches to solve such problems. One employs the constitutive equations valid for arbitrary or, at least, rather wide classes of loading histories. Quasistatic problems for inelastic bodies, specifically beams and plates, were addressed in [77, 81, 82]; and vibration problems for viscoplastic structures in [66, 73, 78, 79].

This approach was used to solve problems for thin-walled structural members (mainly beams) in a practically important formulation that allows for the elastoviscoplasticity and geometrical nonlinearity of the material. Such formulations in combination with well-tested computational schemes allow us to analyze mechanical effects of the interaction of physical and geometrical nonlinearities, specifically snap buckling of initially curved elements [92] and chaotic motions in such elements under harmonic loading [42, 89].

By using exact models under harmonic loading, we can study a number of effects accompanying vibrations such as snap buckling, drift of average plastic strain, dynamic buckling, chaotic motions, etc. Study of such processes is difficult because of

* The study was partially sponsored by the State Fund for Basic Research of the Ministry of Education and Science of Ukraine (Grant No. 01.07/00050).

S. P. Timoshenko Institute of Mechanics, National Academy of Sciences of Ukraine, Kiev. Translated from Prikladnaya Mekhanika, Vol. 40, No. 10, pp. 3–34, September 2004. Original article submitted February 2, 2004.

the severe requirements to the time integration schemes for Cauchy problems. This is due to the stiffness of nonlinear systems describing the plastic transition of the material and the local instability of solutions within internal boundary layers associated with snap buckling of preliminary or plastically curved thin-walled elements [92]. The corresponding findings are generalized in the reviews [67, 83].

The second approach is based on approximate models for specific deformation histories. One of the most important cases is periodic processes excited by harmonic loading. The idea of simplification can be clearly demonstrated by an example of linearly viscoelastic materials. In the case of harmonic deformation, all basic types of constitutive equations—integral (hereditary) or differential—have an algebraic form written in terms of complex stress and strain amplitudes. The relationship between these quantities is expressed in terms of complex moduli [26, 91].

At least two circumstances stimulated efforts to generalize this model to physically nonlinear materials. One is its simplicity due to the absence of the time factor and the other is physical. In some practically important cases, such as internal-friction theory [25, 35–37], the reaction of the material at the frequency of excitation is of primary interest.

In nonlinear damped mechanical systems, single-frequency vibrations occur under moderate loads at resonances. The effective solution of such problems is based on methods of nonlinear mechanics [2].

To study single-frequency vibrations, it is convenient to use the harmonic-linearization method. As applied to continuum mechanics, this method is most fully expounded in [34, 51, 61].

Despite the fact that the single-frequency approximation based on harmonic linearization is well grounded in nonlinear mechanics [2, 38], its practical accuracy should be additionally analyzed for specific classes of problems in the mechanics of nonlinear dissipative media.

The basic question is: Which harmonic-linearization scheme provides the highest accuracy of specific stress–strain characteristics for various classes of nonlinear materials?

The most convincing and justified answer to this question can be obtained by a direct comparison of exact and approximate analyses. The exact analysis is based on the initial inelastic model, and the approximate analysis on its harmonically linearized modification.

Such a comparative analysis was performed in [33] in solving the stress-concentration problem for an elastoplastic cylinder with a cut. Essentially, the approximate model developed there is as follows: consider a body's element within which the hysteresis stress–strain loop is stable under proportional or nearly proportional loading. The governing relations are two equations relating the amplitudes of elastic and plastic strains with the stress amplitudes. The equation parameters are specified based on uniaxial cyclic curves. The maximum stress amplitudes near a cut calculated exactly and by the finite-element method (FEM) are in good agreement.

For elastoplastic bodies, the equations relating the stress and strain amplitudes are independent of the time base of the cycle. They are in particular valid for harmonic loading. For viscoelastic and viscoplastic materials, the amplitude equations should be specified for each specific time base.

The amplitude equations may be different, depending on the norm in which the exact equations are approximated on the class of cyclic, specifically harmonic histories. Within the framework of the classical harmonic-linearization approach, V. A. Pal'mov [34] used approximation in the Hilbert space. The linearizing operator has the form of the differential Voight model, and the norms in which the stiffness and dissipative characteristics of elastoplastic media are approximated are close to the stored and dissipated energies.

A similar scheme and also Galerkin's time scheme were applied to nonlinearly viscoelastic materials in [39, 52–54] and generalized in [51, 61]. The difference between these schemes is in the structure of the final amplitude equations. The Voigt linearization leads to relations similar to the linear viscoelastic equations for harmonic processes (correspondence principle). They are known [26] to be formulated in terms of complex moduli. Thus, the harmonic-linearization scheme leads to a linear–nonlinear analogy. Galerkin's scheme includes weaker constraints than the harmonic-linearization scheme. The corresponding amplitude equations are more general, yet more complex. They contain much more material characteristics.

It is natural to associate the norm in which the complete inelastic operator is approximated with features of the problem. These may be the degree of nonlinearity, the required accuracy of nonlinear stress–strain characteristics responsible for the load-bearing capacity of the structure or the strength of the material, the simplicity of the simplified formulation, etc.

The papers [41, 57, 63, 64] were the first to compare the capabilities of various harmonic-linearization schemes as applied to forced vibrations of nonlinear oscillators as simple resonant systems. The data obtained made it possible to choose the

most accurate harmonic-linearization scheme for nearly simple deformation processes described by generalized flow models such as Bodner–Partom [69], Walker [5], etc.

Later, the simplified model corresponding to this scheme was extended to a wide class of problems on forced stationary vibrations and vibrational heating of spatial and thin-walled elements of homogeneous and piecewise-homogeneous structures. The present review is intended to discuss and generalize the results obtained.

1. Harmonic Deformation of Nonlinearly Dissipative Materials: Monoharmonic Approximation. Consider cyclically stable materials for which the reaction of the stress $\boldsymbol{\sigma}(t)$ to cyclic isothermal strain $\boldsymbol{\epsilon}(\tau)$, $-\infty \le \tau \le t$, $\boldsymbol{\epsilon}(\tau+T)=\boldsymbol{\epsilon}(\tau)$ is a time function of period T. Let us expand the functions $\boldsymbol{\sigma}(t)$ and $\boldsymbol{\epsilon}(t)$ into trigonometric series:

$$\boldsymbol{\sigma}(t)=\overline{\boldsymbol{\sigma}}+\boldsymbol{\sigma}'_1\cos\omega t-\boldsymbol{\sigma}''_1\sin\omega t+\sum_{n=3,5,\ldots}^{\infty}\left(\boldsymbol{\sigma}'_n\cos n\omega t-\boldsymbol{\sigma}''_n\sin n\omega t\right), \tag{1.1}$$

$$\boldsymbol{\epsilon}(t)=\overline{\boldsymbol{\epsilon}}+\boldsymbol{\epsilon}'_1\cos\omega t-\boldsymbol{\epsilon}''_1\sin\omega t+\sum_{n=3,5,\ldots}^{\infty}\left(\boldsymbol{\epsilon}'_n\cos n\omega t-\boldsymbol{\epsilon}''_n\sin n\omega t\right), \tag{1.2}$$

where $\boldsymbol{\sigma}'_n$, $\boldsymbol{\sigma}''_n$, and $\boldsymbol{\epsilon}'_n$, $\boldsymbol{\epsilon}''_n$, $n=1, 3, 5, \ldots$, are the stress and strain amplitudes, and $\overline{\boldsymbol{\sigma}}$ and $\overline{\boldsymbol{\epsilon}}$ are the average stress and strain components, respectively.

The amplitudes $\boldsymbol{\sigma}'_n$, $\boldsymbol{\sigma}''_n$ and $\boldsymbol{\epsilon}'_n$, $\boldsymbol{\epsilon}''_n$ are time independent in the case of steady periodic vibration and are functions of period number in the case of transient. Then the properties of the material are completely characterized by the relationship between the amplitudes of stress harmonics and strain amplitudes.

Monoharmonic approximation is called the sum of the first three terms in expressions (1.1) and (1.2) that determine the response of the system at the frequency of excitation, with the other terms neglected. Then we have

$$\boldsymbol{\sigma}(\tau)=\overline{\boldsymbol{\sigma}}+\boldsymbol{\sigma}'\cos\omega\tau-\boldsymbol{\sigma}''\sin\omega\tau, \qquad \boldsymbol{\sigma}',\boldsymbol{\sigma}'',\overline{\boldsymbol{\sigma}}=\text{const}, \tag{1.3}$$

$$\boldsymbol{\epsilon}(\tau)=\overline{\boldsymbol{\epsilon}}+\boldsymbol{\epsilon}'\cos\omega\tau-\boldsymbol{\epsilon}''\sin\omega\tau, \qquad \theta(\tau)=\overline{\theta}, \qquad \boldsymbol{\epsilon}',\boldsymbol{\epsilon}',\overline{\boldsymbol{\epsilon}},\overline{\theta}=\text{const}, \qquad -\infty\le\tau\le t. \tag{1.4}$$

Here either $\boldsymbol{\epsilon}(t)$ or $\boldsymbol{\sigma}(t)$ may be controllable; then the other quantity would be the reaction of the material.

Choosing the strain to be controllable and taking (1.3) and (1.4) into account, we arrive at the constitutive equations for monoharmonic approximation

$$\overline{\boldsymbol{\sigma}}=\hat{\overline{\boldsymbol{\sigma}}}\left(\overline{\boldsymbol{\epsilon}},\boldsymbol{\epsilon}',\boldsymbol{\epsilon}'',\omega\right), \qquad \boldsymbol{\sigma}'=\hat{\boldsymbol{\sigma}}'\left(\overline{\boldsymbol{\epsilon}},\boldsymbol{\epsilon}',\boldsymbol{\epsilon}'',\omega\right), \qquad \boldsymbol{\sigma}''=\hat{\boldsymbol{\sigma}}''\left(\overline{\boldsymbol{\epsilon}},\boldsymbol{\epsilon}',\boldsymbol{\epsilon}'',\omega\right), \tag{1.5}$$

where $\hat{\overline{\boldsymbol{\sigma}}}$, $\hat{\boldsymbol{\sigma}}'$, and $\hat{\boldsymbol{\sigma}}''$ are symmetric tensor functions of the arguments specified in brackets.

By virtue of (1.5), temperature is not considered, whenever possible.

The amplitude equations (1.5) have two interpretations [40]:

(i) There are several ways of deriving the monoharmonic-approximation equations (1.5) from the complete constitutive equations. The choice of one linearization scheme or another is dictated by the properties of the mechanical system and the objective of research.

(ii) Relations (1.5) can be specified based on direct experiments, without resort to any complete constitutive equations.

These interpretations were formally analyzed in [51].

2. Harmonic-Linearization Method. Standard Scheme [12, 34, 43, 48, 57]. Let the stress deviator $\boldsymbol{s}(t)$ be a nonlinear isotropic functional of the complete prehistory of the strain deviator $\boldsymbol{e}(\tau)$, $-\infty<\tau<t$,

$$\boldsymbol{s}(t)=\mathop{\boldsymbol{s}}_{\tau=-\infty}^{t}\left[\boldsymbol{e}(\tau)\right]. \tag{2.1}$$

Let us consider harmonic strain histories

$$\boldsymbol{e}(\tau)=\boldsymbol{e}'\cos\omega\tau-\boldsymbol{e}''\sin\omega\tau, \qquad -\infty<\tau<t, \tag{2.2}$$

where $\boldsymbol{e}'$ and $\boldsymbol{e}''$ are amplitudes, and ω is frequency.

To approximate functional (2.1) on the strain histories (2.2), we will use the harmonic-linearization method and the Voight equation [34, 38]

$$\underset{\tau=-\infty}{\overset{t}{\boldsymbol{s}}}\left[e(\tau)\right]\approx 2G'\boldsymbol{e}+2\omega^{-1}G''\dot{\boldsymbol{e}}, \tag{2.3}$$

where G' and G'' are scalar coefficients, and $\dot{\boldsymbol{e}}=\partial\boldsymbol{e}/\partial t$.

These coefficients are determined from the minimum condition for the root-mean-square error of approximation (1.3) on the monoharmonic strain histories (1.2)

$$R=\left\langle(\boldsymbol{s}-2G'\boldsymbol{e}-2\omega^{-1}G''\dot{\boldsymbol{e}})\cdot(\boldsymbol{s}-2G'\boldsymbol{e}-2\omega^{-1}G''\dot{\boldsymbol{e}})\right\rangle=\min, \tag{2.4}$$

where $\langle f(t)\rangle=\dfrac{1}{T}\int\limits_0^T f(\tau)d\tau$ is averaging over the period T, and $\boldsymbol{a}\cdot\boldsymbol{b}$ is the convolution of two tensors.

Minimizing the function R,

$$\partial R/\partial G'=0,\quad \partial R/\partial G''=0, \tag{2.5}$$

and resolving these equations for G' and G'', we obtain

$$G'=\langle\boldsymbol{s}(\boldsymbol{e}(\tau))\cdot\boldsymbol{e}\rangle/2e_i^2,\quad G''=\langle\boldsymbol{s}(\boldsymbol{e}(\tau))\cdot\dot{\boldsymbol{e}}\rangle/2\omega e_i^2, \tag{2.6}$$

where e_i is the intensity of shear strain amplitudes, $e_i^2=(\boldsymbol{e}'\cdot\boldsymbol{e}'+\boldsymbol{e}''\cdot\boldsymbol{e}'')/2$.

The coefficients G' and G'' are functions of $\boldsymbol{e}'$, $\boldsymbol{e}''$, ω, and θ.

Applying the single-frequency approximation (1.2) $\boldsymbol{s}(t)=\boldsymbol{s}'\cos\omega t-\boldsymbol{s}''\sin\omega t$ to the stresses and substituting it into (2.3), we arrive at equations for the amplitudes:

$$\boldsymbol{s}'=2G'\boldsymbol{e}'-2G''\boldsymbol{e}'',\quad \boldsymbol{s}''=2G''\boldsymbol{e}'+2G'\boldsymbol{e}''. \tag{2.7}$$

Relations (2.7) can be represented in a complex form:

$$\tilde{\boldsymbol{s}}=2\tilde{G}\tilde{\boldsymbol{e}}, \tag{2.8}$$

where $\tilde{G}=G'+iG''$ is the complex shear modulus; and $\tilde{\boldsymbol{s}}$ and $\tilde{\boldsymbol{e}}$ are the complex stress and strain amplitudes, $\tilde{\boldsymbol{s}}=\boldsymbol{s}'+i\boldsymbol{s}''$, $\tilde{\boldsymbol{e}}=\boldsymbol{e}'+i\boldsymbol{e}''$.

The dependence of G' and G'' on $\boldsymbol{e}'$ and $\boldsymbol{e}''$ in the isotropic tensor-linear functionals (2.1) is realized in terms of a set of invariants $\boldsymbol{e}'\cdot\boldsymbol{e}'$, $\boldsymbol{e}'\cdot\boldsymbol{e}''$, and $\boldsymbol{e}''\cdot\boldsymbol{e}''$ [61].

In the case of proportional (monophase) harmonic deformation, the dependence of G' and G'' on $\boldsymbol{e}'$ and $\boldsymbol{e}''$ becomes much simpler:

$$G'=G'(e_i),\quad G''=G''(e_i). \tag{2.9}$$

The inelastic strains $\boldsymbol{\epsilon}^p$ are very important for materials described by generalized flow models. This is because a number of low-cycle fatigue criteria, specifically the Coffin–Manson criterion [75], are formulated in terms of inelastic strain amplitudes (ranges).

To determine them, the relation for $\boldsymbol{\epsilon}^p$ is harmonically linearized in addition to Eq. (1.1):

$$\boldsymbol{\epsilon}^p(t)=\underset{\tau=-\infty}{\overset{t}{\boldsymbol{\epsilon}^p}}\left[\boldsymbol{e}(\tau)\right]. \tag{2.10}$$

A differential Voigt-type functional is also used for approximation:

$$\underset{\tau=-\infty}{\overset{t}{\boldsymbol{\epsilon}^p}}\left[\boldsymbol{e}(\tau)\right]\approx\hat{\boldsymbol{\epsilon}}^p(t)=\lambda'\boldsymbol{e}(t)+\lambda''\omega^{-1}\dot{\boldsymbol{e}}(t). \tag{2.11}$$

By analogy with stresses, we arrive at a complex equation for amplitudes [47, 48]:

$$\tilde{\boldsymbol{\epsilon}}^p = \tilde{\lambda}\tilde{\boldsymbol{e}}, \tag{2.12}$$

where $\tilde{\lambda}$ is the complex plastic coefficient, $\tilde{\lambda} = \lambda' - i\lambda''$.

It is a matter of direct verification to show that the approximate equations (2.3) in the harmonic-linearization scheme are equivalent to the complete equation (2.1) for the two quantities Π_s and D'_s:

$$\Pi_s = \langle \boldsymbol{s} \cdot \boldsymbol{e} \rangle = \frac{1}{2}(\boldsymbol{s}' \cdot \boldsymbol{e}' + \boldsymbol{s}'' \cdot \boldsymbol{e}''), \quad D'_s = \langle \boldsymbol{s} \cdot \dot{\boldsymbol{e}} \rangle = \frac{1}{2}(\boldsymbol{s}' \cdot \boldsymbol{e}'' - \boldsymbol{s}'' \cdot \boldsymbol{e}'). \tag{2.13}$$

The former (Π_s) may be regarded as a parameter reflecting the period-average or maximum stored energy [55]. In a steady-state periodic process, D'_s is equal to the period-average energy dissipation rate [61]. Thus, the standard linearization scheme leads to a monoharmonic model equivalent to the exact energy model.

3. Modified Harmonic-Linearization Scheme [47, 48]. An analysis of the complex characteristics obtained by the standard harmonic-linearization scheme shows that the loss moduli G'' and λ'' are determined by the period-average dissipation rate. However, the above energy method of determining G' and λ' does not allow calculating the exact amplitudes (ranges) of stresses and inelastic strains in a cycle.

The accuracy of the calculated stresses $\boldsymbol{s}$ and inelastic strains $\boldsymbol{\epsilon}^p$ can be increased by using a different approach to the determination of the moduli G' and λ'. For simplicity, we will restrict ourselves to the case of proportional loading. Let us determine the amplitudes of the deviatoric stresses, total and inelastic strains

$$\begin{bmatrix} \Delta\boldsymbol{s} \\ \Delta\boldsymbol{\epsilon} \\ \Delta\boldsymbol{\epsilon}^p \end{bmatrix} = \max_T \begin{bmatrix} \boldsymbol{s}(t) \\ \boldsymbol{\epsilon}(t) \\ \boldsymbol{\epsilon}^p(t) \end{bmatrix} - \min_T \begin{bmatrix} \boldsymbol{s}(t) \\ \boldsymbol{\epsilon}(t) \\ \boldsymbol{\epsilon}^p(t) \end{bmatrix} \tag{3.1}$$

and the corresponding intensities

$$s_i^2 = \frac{1}{8}\Delta\boldsymbol{s} \cdot \Delta\boldsymbol{s}, \quad e_i^2 = \frac{1}{8}\Delta\boldsymbol{e} \cdot \Delta\boldsymbol{e}, \quad \varepsilon_i^{p2} = \frac{1}{8}\Delta\boldsymbol{\epsilon}^p \cdot \Delta\boldsymbol{\epsilon}^p. \tag{3.2}$$

Consider cyclic diagrams designed by the exact model,

$$s_i = s_i(e_i, \omega), \quad \varepsilon_i^p = \varepsilon_i^p(e_i, \omega). \tag{3.3}$$

Each of them is the dependence of the amplitude of reaction intensity on the intensity of stationary excitation at prescribed frequency.

In view of (2.10) and (2.12), such diagrams obtained by the approximate model have the form

$$\hat{s}_i = 2|\tilde{G}|\, e_i, \quad \hat{\varepsilon}_i^p = |\tilde{\lambda}|\, e_i. \tag{3.4}$$

In essence, the modification of the model is as follows. The expressions for G'' and λ'' remain the same:

$$\langle D' \rangle = \langle \boldsymbol{s} \cdot \dot{\boldsymbol{e}} \rangle = \omega G''(e_i, \omega)\, e_i = \omega G \lambda''(e_i, \omega)\, e_i, \tag{3.5}$$

where G is the shear modulus.

The moduli G' and λ' are calculated from the condition that the approximate model exactly satisfies the corresponding cyclic diagrams $\hat{s}_i \equiv s_i$ and $\hat{\varepsilon}_i^p \equiv \varepsilon_i^p$:

$$G'(e_i, \omega) = \left[\frac{s_i^2(e_i, \omega)}{4e_i^2} - G''^2(e_i, \omega)\right]^{1/2}, \quad \lambda'(e_i, \omega) = \left[\frac{\varepsilon_i^{p^2}(e_i, \omega)}{e_i^2} - \lambda''^2(e_i, \omega)\right]^{1/2}, \tag{3.6}$$

where $s_i^2 = (\boldsymbol{s}' \cdot \boldsymbol{s}' + \boldsymbol{s}'' \cdot \boldsymbol{s}'')/2$.

Thus, according to (3.5) and (3.6), the complex characteristics of monoharmonic approximation are determined from the equations

$$|\tilde{G}| = \frac{s_i}{2e_i}, \quad G'' = \frac{1}{\omega e_i^2}\langle \boldsymbol{s}\cdot\boldsymbol{e}\rangle, \quad |\tilde{\lambda}| = \frac{\varepsilon_i^p}{e_i}, \quad \lambda'' = \frac{G''}{G} \tag{3.7}$$

and reflect the essence of the modified harmonic-linearization model.

4. Mathematical Aspects. Let the stress $\boldsymbol{s}(t)$ and inelastic strain $\boldsymbol{\epsilon}^p(t)$ on arbitrary histories $\boldsymbol{e}(\tau)$, $-\infty < \tau < t$, be defined by

$$\boldsymbol{s}(t) = \overset{t}{\underset{\tau=-\infty}{\boldsymbol{s}}}\left[\boldsymbol{e}(\tau)\right], \quad \boldsymbol{\epsilon}^p(t) = \overset{t}{\underset{\tau=-\infty}{\boldsymbol{\epsilon}^p}}\left[\boldsymbol{e}(\tau)\right], \quad -\infty < t < \infty. \tag{4.1}$$

Consider the approximation of these functionals on harmonic histories:

$$\boldsymbol{e}(\tau) = \mathrm{Re}\left(\tilde{\boldsymbol{e}}e^{i\omega\tau}\right) = e'\cos\omega\tau - e''\sin\omega\tau. \tag{4.2}$$

We will restrict ourselves to the oscillating components $\boldsymbol{s}(t)$ and $\boldsymbol{\epsilon}^p(t)$ defined by (4.1).

Denote by S a set of T-periodic functions $\boldsymbol{s}(t)$, $\boldsymbol{s}(t) = \boldsymbol{s}(t+T)$, defined by (4.1). According to [51], the energies Π_s and D'_s defined by (2.13) are assumed to be nonnegative: $\Pi_s \ge 0$, $D'_s \ge 0$.

Let us define energy norms in the space S:

$$||s||_{\Pi_s} = \int_0^T \boldsymbol{s}(t)\cdot\boldsymbol{e}(t)\,dt, \quad ||s||_{D'_s} = \int_0^T \boldsymbol{s}(t)\cdot\dot{\boldsymbol{e}}(t)\,dt, \tag{4.3}$$

and the Hilbert norm $||s||_{L_2} = \langle \boldsymbol{s}^2(t)\rangle$.

Relation (2.4) is the requirement that the difference $\boldsymbol{s}(t) - \hat{\boldsymbol{s}}(t)$ be minimum in the norm of the space L_2. Equation (2.5) following from (2.4), (2.6) means zero differences of stresses in energy norms (4.3).

To analyze the inelastic strain using generalized flow models, we will consider the following equation rather than Eq. (2.1):

$$\boldsymbol{s}(t) = 2G\left(\boldsymbol{\epsilon}(t) - \boldsymbol{\epsilon}^p(t)\right) \tag{4.4}$$

and the flow rule (2.10). Let us introduce the integrals

$$\Pi_\varepsilon = \int_0^T \boldsymbol{\epsilon}^p(t)\cdot\boldsymbol{e}(t)\,dt, \quad D'_\varepsilon = -\int_0^T \boldsymbol{\epsilon}^p(t)\cdot\dot{\boldsymbol{e}}(t)\,dt \tag{4.5}$$

and establish whether they are positive. Convoluting (4.4) term by term with the tensors $\boldsymbol{e}(t)$ and $\dot{\boldsymbol{e}}(t)$, taking (2.7) into account, and performing some transformations, we obtain

$$\Pi_\varepsilon = 2G\left(1 - \frac{G'}{G}\right)e_i^2, \quad D'_\varepsilon = \frac{1}{2}\langle \boldsymbol{s}\cdot\dot{\boldsymbol{e}}\rangle. \tag{4.6}$$

The inequality $\Pi_\varepsilon > 0$ follows from the estimate $G' \le G$ for materials with soft nonlinearity, i.e., for most viscoelastoplastic materials. The right-hand side of the second equality in (4.6) is the period-average dissipation rate. Therefore, $D'_\varepsilon \ge 0$ according to the second law of thermodynamics [62].

Hence, based on (4.5) we can determine the norms in the space of T-periodic functions $\boldsymbol{\epsilon}^p(t)$:

$$\Pi_\varepsilon = ||\varepsilon^p||_{\Pi_\varepsilon}, \quad D'_\varepsilon = ||\varepsilon^p||_{D'_\varepsilon}. \tag{4.7}$$

By analogy with stresses, we establish a zero error of approximation of inelastic strains in quasienergy norms (4.7).

The parameters of the modified model are determined using two norms. Introduce a Banach space of continuous, on [0; T], functions $f(t)$ with zero mean and norm

$$||f(t)||_B = \max_{[0;T]} f(t) - \min_{[0;T]} f(t).$$

It is obvious that the first and third relations in (3.7) are equivalent to

$$||\boldsymbol{s}(t)||_B = ||\hat{\boldsymbol{s}}(t)||_B, \quad ||\boldsymbol{\epsilon}^p(t)||_B = ||\hat{\boldsymbol{\epsilon}}^p(t)||_B.$$

The second and fourth equalities in (3.7) follow from the condition of equality of period-average dissipation rates, as in the standard model. This, according to (4.7), is equivalent to zero deviations of stresses and inelastic strains in dissipative norms

$$||\boldsymbol{s}(t)||_{D_s'} = ||\hat{\boldsymbol{s}}(t)||_{D_s'}, \quad ||\boldsymbol{\epsilon}^p(t)||_{D_\varepsilon'} = ||\hat{\boldsymbol{\epsilon}}^p(t)||_{D_\varepsilon'}.$$

5. Mechanical Features of Various Harmonic-Linearization Schemes. Let us compare the above-mentioned two harmonic-linearization schemes by an example of the generalized Bodner–Partom flow model [69] with thermal recovery disregarded.

For the case of shear (torsion), the Bodner–Partom model includes the following equations:

Hooke's law

$$s = 2G(e - \varepsilon^p), \tag{5.1}$$

the flow rule

$$\dot{\varepsilon}^p = D_0 \exp\left[-\frac{1}{2}\left(\frac{K+D}{\sqrt{3}\,|s|}\right)^{2n}\right]\frac{s}{|s|}, \quad \varepsilon^p(0) = 0, \tag{5.2}$$

the equation for the scalar isotropic-hardening parameter K

$$\dot{K} = m_1(K_1 - K)\dot{W}^p, \quad K(0) = K_0, \tag{5.3}$$

the evolution equation for the kinematic-hardening parameter β

$$\dot{\beta} = m_2\,(D_1 s/|s| - \beta)\dot{W}^p, \quad \beta(0) = 0, \tag{5.4}$$

where D_0, D_1, n, m_1, m_2, K_0, and K_1 are the model parameters determined experimentally; and $\dot{W}^p$ is plastic capacity, $\dot{W}^p = 2s\dot{\varepsilon}^p$.

Processing the experimental data from [1] for AMg-6 aluminum alloy by the method from [58] produces the following model parameters:

$$\begin{gathered} D_0 = 10^4\ \text{sec}^{-1}, \quad K_0 = 323.6\ \text{MPa}, \quad K_1 = 647.4\ \text{MPa}, \\ n = 2.06, \quad m_1 = 0.182\ \text{MPa}, \quad m_2 = 0, \quad G = 3.044 \cdot 10^4\ \text{MPa}. \end{gathered} \tag{5.5}$$

The cyclic characteristics have been calculated for deformation histories $e = e_0 \sin \omega t$.

Figure 5.1 shows a cyclic curve (line *1*) for standard monoharmonic approximation $|\tilde{s}| \sim e_0$, $|\tilde{s}| = 2|\tilde{G}|\,e_0$ and the exact cyclic curve (line *2*) $\Delta s/2 \sim e_0$ plotted by numerical integration of system (5.1)–(5.4) for frequency $\omega = 2\pi\ \text{sec}^{-1}$. Also, the figure shows the approximate $|\tilde{\varepsilon}^p| \sim e_0$, $|\tilde{\varepsilon}^p| = 2|\tilde{\lambda}|\,e_0$ (line *3*) and exact cyclic $\Delta\varepsilon^p/2 \sim e_0$ (line *4*) curves for inelastic strain. Curve *5* represents monotonic torsion with constant velocity $\dot{e}_0$ = 0.1 sec^{-1} (static diagram). It is seen that the standard harmonic-linearization model produces strongly overestimated amplitudes (ranges) of stresses and inelastic strains. It is obvious that the cyclic curves generated by the modified model coincide with the exact curves because the latter are incorporated in the basic relations (3.6) for the components G' and λ' of the complex moduli $\tilde{G}$ and $\tilde{\lambda}$.

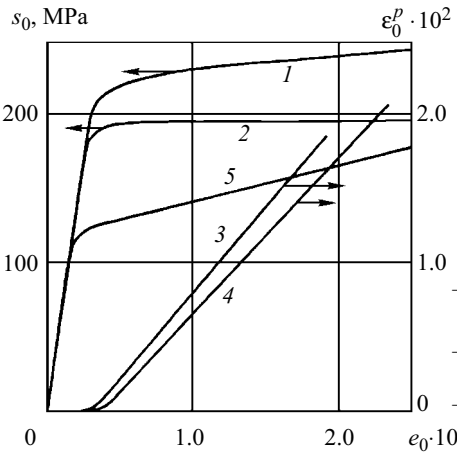

Fig. 5.1

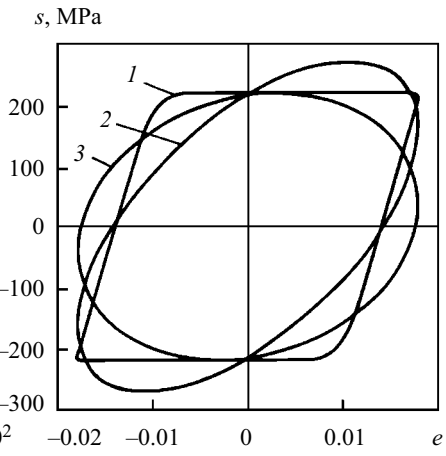

Fig. 5.2

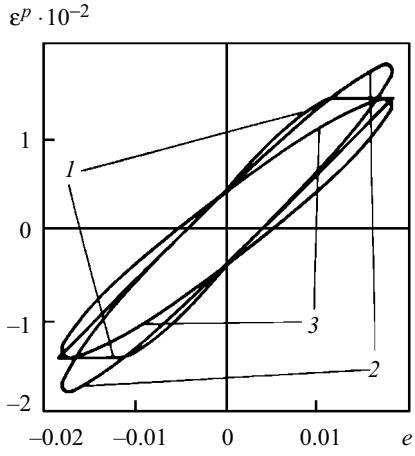

Fig. 5.3

Figure 5.2 clearly demonstrates the difference between the approximate approaches for $e_0 = 1.8 \cdot 10^{-2}$ and $\omega = 2\pi$ sec^{-1}. Curves *1–3* are the hysteresis loops s versus e for the exact, standard, and modified models, respectively. Figure 5.3 shows similar loops (ε^p versus e) for inelastic strain. When the areas of all the loops are equal (i.e., they are equivalent in dissipation over the period), the modified and exact models produce equal amplitudes of stress and inelastic strain.

Note that it is very important to associate the coefficient $\tilde{\lambda}$ with the exact cyclic curve ε^p versus e in order to evaluate low-cycle fatigue based on criteria for amplitudes of inelastic strain such as the Coffin–Manson equation [75] $(\Delta\varepsilon^p) N_f^b = \text{const}$, where p and b are constants, and N_f is the number of cycles to failure.

Figure 5.4a shows the deformation dependences of the moduli $G'(e_0)$ and $G''(e_0)$ at frequency $\omega = 2\pi$ sec^{-1}. Curves *1* and *2* represent the modulus G' calculated by the standard and modified models, respectively. Curve *3* represents the modulus G'' identical for both models. The standard model overestimates the cyclic stiffness of the material. It is seen that below the cyclic plastic limit, $e_T \cong 0.003$, the material behaves as an elastic body; and when $e > e_T$, the stiffness modulus G' abruptly decreases and the loss modulus G'' abruptly increases with increasing e. The inelastic strain varies nearly linearly: $e^p / 2 = e - e_T$. Thus, the cyclic behavior of the material is essentially nonlinear.

The mechanical interpretation of the two schemes includes two aspects.

First, the stress amplitude in the standard model is the coefficient of the principal harmonic in the Fourier series of the function $\boldsymbol{s}(t)$. The stress amplitude in the modified model, however, is assumed equal to the exact stress amplitude and carries information on all the Fourier harmonics.

Second, the cyclic diagram s_i versus e_i in the standard model represents the principal harmonic of the stress amplitude, whereas the analogous curve in the modified model coincides with the experimental curve from [28].

Note also that the differences between the two schemes established above do not give a comprehensive idea of the accuracy of monoharmonic approximation in general and of each of the schemes in particular. Such an idea can be gained by comparing the solutions of specific classes of problems obtained based on the exact and each of the approximate models.

6. Generalization of the Approximate Model to Nonstationary Harmonic Deformation [43, 44, 47, 97]. Relations (3.6) and (3.7) determine the parameters of the modified model for stationary vibrations. Let us consider the case where the intensity amplitudes vary during cycle stabilization under harmonic loading. According to the harmonic-linearization method, the complex amplitudes of the strain, inelastic strain, and stress deviators are related in the Nth cycle via the complex shear modulus $\tilde{G}_N$, $\tilde{G}_N = G'_N + iG''_N$, and the inelasticity coefficient $\tilde{\lambda}_N$, $\tilde{\lambda}_N = \lambda'_N - i\lambda''_N$,

$$\tilde{\boldsymbol{s}}_N = 2\tilde{G}_N \tilde{\boldsymbol{e}}_N, \quad \tilde{\boldsymbol{\epsilon}}_N^p = \tilde{\lambda}_N \tilde{\boldsymbol{e}}_N, \quad N = 1, 2, 3, \ldots, \tag{6.1}$$

where, as before, $\tilde{G}_N$ and $\tilde{\lambda}_N$ for proportional loading are functions of the strain intensity, frequency of vibrations, and temperature

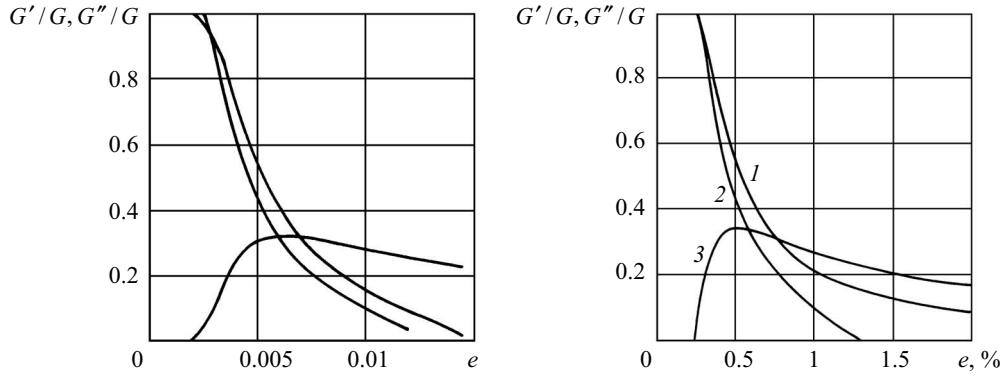

Fig. 5.4

$$\widetilde{G}_N = \widetilde{G}_N\left(e_{iN}, \omega, \theta\right), \quad \widetilde{\lambda}_N = \widetilde{\lambda}_N\left(e_{iN}, \omega, \theta\right). \tag{6.2}$$

For the standard model, the components of the complex characteristics $\widetilde{G}_N$ and $\widetilde{\lambda}_N$ are defined by

$$e_N = e_0,$$

$$\begin{bmatrix} G'_N \\ G''_N \end{bmatrix} = \frac{1}{2e_0}\begin{bmatrix} s''_N \\ -s'_N \end{bmatrix}, \quad \begin{bmatrix} s'_N \\ s''_N \end{bmatrix} = \left\langle \sigma(t)\begin{bmatrix} \cos\omega t \\ -\sin\omega t \end{bmatrix} \right\rangle_N, \quad s_N = \left(s'^2_N + s''^2_N\right)^{1/2},$$

$$\lambda'_N = 1 - \frac{G'_N}{G}, \quad \lambda''_N = \frac{G''_N}{G}, \tag{6.3}$$

where $\langle(\cdot)\rangle_N = \dfrac{1}{T}\displaystyle\int_{(N-1)T}^{NT} (\cdot)\, dt.$

For the modified model, the complex moduli are calculated by formulas (3.6) and (3.7). For example, in the Nth strain-controlled cycle, the imaginary parts of the moduli are defined by

$$e_N = e_0,$$

$$\langle D' \rangle_N = \langle \boldsymbol{s} \cdot \dot{\boldsymbol{\varepsilon}}^p \rangle_N = \langle \boldsymbol{s} \cdot \dot{\boldsymbol{e}} \rangle_N = \omega G''_N e_0^2 = \omega \lambda''_N e_0^2 G,$$

$$\frac{s_N}{e_0} = 2\left|\widetilde{G}_N\right|, \quad \frac{\varepsilon^p_N}{e_0} = \left|\widetilde{\lambda}_N\right|, \tag{6.4}$$

where $\left|\widetilde{G}_N\right| = \left(G'^2_N + G''^2_N\right)^{1/2}$, $\left|\widetilde{\lambda}_N\right| = \left(\lambda'^2_N + \lambda''^2_N\right)^{1/2}$.

In the modified monoharmonic-approximation (MHA) model, the moduli G'_N and λ'_N are determined from the cyclic diagrams (3.3). Let $s_{iN} = s_{iN}(e_0, \omega)$ and $\varepsilon^p_{iN} = \varepsilon^p_{iN}(e_0, \omega)$ be generalized diagrams that express the dependence of the amplitudes of stress and inelastic-strain intensities on the intensity e_0 in the Nth cycle. Obviously, for cyclically stable materials, the relations $s_{iN}(e_0) \to s_i(e_0)$ and $\varepsilon^p_{iN}(e_0) \to \varepsilon^p_i(e_0)$ are valid for sufficiently large N.

Typical diagrams for AMg-6 aluminum alloy at f = 1 Hz are shown in Fig. 6.1.

Generalizing Eqs. (3.6) and (3.7), we determine the characteristics in the Nth cycle as follows:

$$G''_N\left(e_i, \omega\right) = \frac{\langle D' \rangle_N}{\omega e_i^2}, \quad \lambda''_N\left(e_i, \omega\right) = \frac{G''_N\left(e_i, \omega\right)}{G},$$

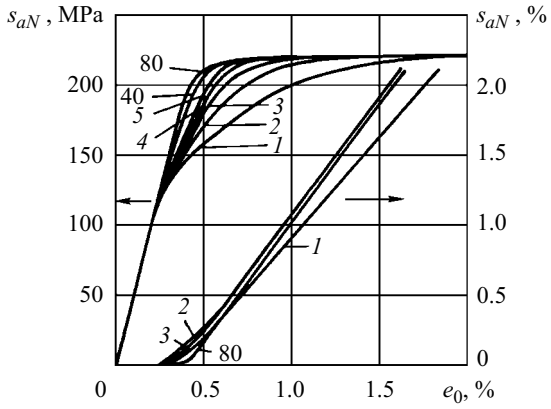

Fig. 6.1

$$G'(e_i,\omega)=\left[\frac{s_i^2(e_i,\omega)}{4e_i^2}-G''^2(e_i,\omega)\right]^{1/2},$$

$$\lambda'(e_i,\omega)=\left[\frac{\varepsilon_i^{p^2}(e_i,\omega)}{e_i^2}-\lambda''^2(e_i,\omega)\right]^{1/2}. \qquad (6.5)$$

Thus, the nonstationary model contains $3N$ functions of e_i and ω.

7. Nonlinearly Viscoelastic Oscillator [41, 64]. An important problem used to test various models and solution methods is a nonlinear oscillator at resonance [2].

Consider a shear oscillator, i.e., a mass M suspended from a nonlinear viscoelastic spring (Fig. 7.1). The mechanical behavior of the spring is described by the nonlinear model of standard viscoelastic body [26], where the tangential stress s and shear strain e are related by

$$s=2G_0(e-e_v), \qquad \dot{e}_v=\frac{1}{2\eta}(s-2G_1e_v), \qquad e_v(0)=0, \qquad (7.1)$$

where G_0 is the instantaneous modulus, and e_v is the viscous strain component. The nonlinear properties of the model are defined by

$$G_1=G_{01}\exp(-e_0|e_v|^{\gamma}), \qquad \eta=\eta_0\exp(-\dot{e}_0|\dot{e}_v|^{\beta}), \qquad (7.2)$$

where G_{01}, η_0, e_0, $\dot{e}_0$, γ, and β are the model parameters, and e_0, $\dot{e}_0$, γ, and β characterize the degree of nonlinearity.

The vibrations of a mass M on a vibration shear isolator of area F and height H (Fig. 7.1) are described by the equation

$$M\ddot{x}+sF=Fs_0\sin\omega t, \qquad x(0)=0, \qquad \dot{x}(0)=0, \qquad (7.3)$$

where s_0 is the external shear load divided by the area of the vibration isolator, and ω is the frequency of loading.

In view of (7.1), Eq. (7.3) takes the form

$$\ddot{e}+\omega_0^2(e-e_v)=\omega_0^2e_0^*\sin\omega t, \qquad e(0)=\dot{e}(0)=0, \qquad (7.4)$$

where $e=x/2H$, $\omega_0^2=G_0F/HM$, and $e_0^*=s_0/2G_0$.

Relations (7.1) and (7.4) form a closed-form system of equations for e, s, and $\dot{e}_v$. An approximate formulation for the single-frequency vibrations of the mass results from applying the harmonic-linearization schemes described above. As a result, we arrive at the following equations for the amplitude e and phase φ of forced steady vibrations:

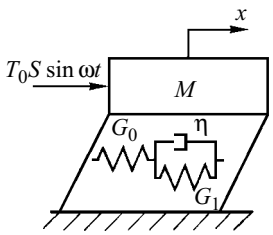

Fig. 7.1

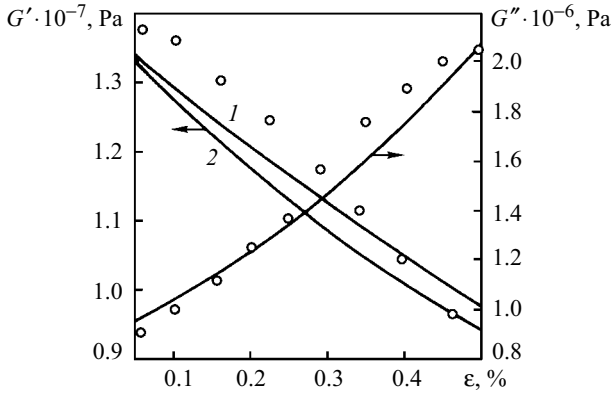

Fig. 7.2

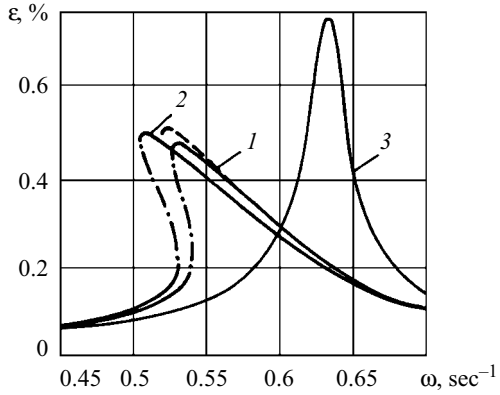

Fig. 7.3

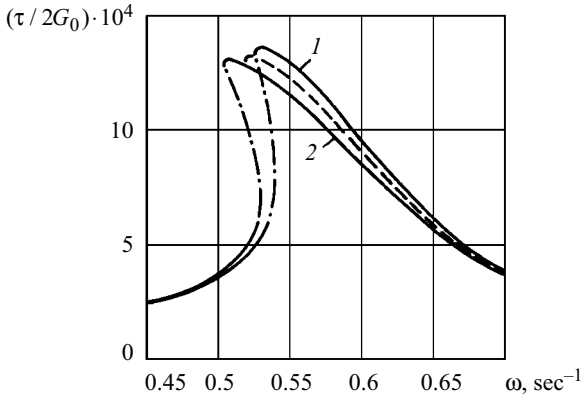

Fig. 7.4

$$e_0^* - \left[(\hat{G}' - \omega^2/\omega_0^2)^2 + \hat{G}''^2\right]^{-1/2} = 0, \quad \varphi = (\hat{G}' - \omega^2/\omega_0^2)/\hat{G}'', \tag{7.5}$$

where $\hat{G}' = G'/G_0$ and $\hat{G}'' = G''/G_0$ are the normalized components of the complex shear modulus.

The vibration isolator is made of butyl rubber (+28% of black). Processing the experimental data from [88], we obtain the following parameters of model (7.1), (7.2):

$$G_0 = 3.45\cdot10^7 \text{ Pa},\ G_{01} = 23\cdot10^6 \text{ Pa},\ \eta_0 = 2.462\cdot10^6 \text{ Pa·sec},\ e_0 = 95.8,\ \gamma = 0.89,\ \dot{e}_0 = 327,\ \beta = 1.12. \tag{7.6}$$

The solid lines in Fig. 7.2 are the deformation dependences of G' and G'' calculated for the parameters (7.6). The open circles stand for the experimental data. Figures 1 and 2 show the modulus G' calculated by the standard and modified linearization schemes. It is seen that the material behaves as a nonlinear body over the entire interval of deformation; and G' decreases and G'' increases with increasing strain.

Figures 7.3 and 7.4 show resonant amplitude–frequency curves for the displacements of the mass and the forces in the vibration isolator, respectively, under load $e_0^* = 0.12\cdot10^{-3}$. The dashed curves have been calculated by direct numerical integration of the original equations (7.1) and (7.4) over time by the implicit Euler method. The system of nonlinear equations generated at each time step was solved by the method of successive iteration with Steffensen–Aitken convergence acceleration [65]. Curves *1* and *2* refer to the standard and modified approaches. Curve *3* in Fig. 7.3 is the linearly viscoelastic characteristic ($e_0 = \dot{e}_0 = 0$).

It is seen that within a certain frequency range the standard model is in good agreement with the exact (numerical) solution in kinematic quantities, yet is inferior to the modified approach in estimating the maximum displacement of the mass in the resonance domain. These models yield the upper and lower bounds for the stress amplitudes in the vibration isolator, respectively. As with the displacements, the modified model produces an exacter value of the maximum stress amplitude.

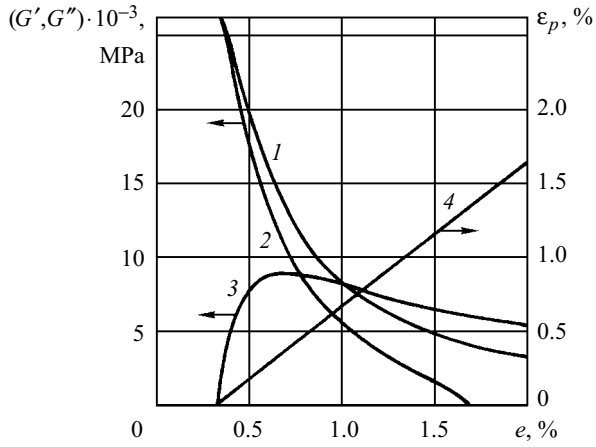

Fig. 8.1

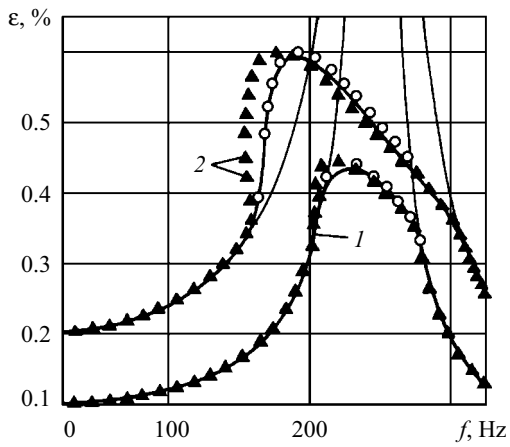

Fig. 8.2

By and large, the results demonstrate that both harmonic-linearization schemes supplement each other and, when used together, allow describing the strain and stress resonance characteristics of vibrating systems containing nonlinearly viscoelastic vibration isolators.

Calculations show that when loads cause a total strain up to 2%, the contribution of higher harmonics to the total amplitude of vibrations is no greater than 6%. Thus, the use of the MHA model under the conditions of not very strong nonlinearity leads to just a minor error.

8. Oscillator with an Element Described by the Generalized Flow Model [63]. Consider a shear oscillator (Fig. 7.1) whose damping element is described by the system of equations (5.1)–(5.4) with parameters (5.5). The vibration equation still has the form (7.3).

Figure 8.1 shows the calculated components of the complex modulus for the deformation cycle at frequency $f = 243$ Hz. Curves *1* and *2* are the strain-dependences of G' for the standard and modified models, respectively; curve *3* represents the modulus G'' equal for both models; and curve *4* is the diagram $\Delta e^p(\omega, e)$.

Figure 8.2 shows the frequency dependences of the amplitudes of the total strain e, plastic strain e^p, and stresses at linear resonance frequency $f_0 = 243$ Hz. Similar curves for inelastic strain and stress are demonstrated in Figs. 8.3 and 8.4. Curves *1* and *2* correspond to $e_0^* = 0.1\cdot 10^{-2}$ and $0.2\cdot 10^{-2}$, respectively. The solid lines have been obtained by direct integration of problem (5.1)–(5.4), (7.4) over time. The open circles and triangles stand for the results obtained by the standard and modified models. The thin lines represent the linearly elastic problem. It is seen that the resonance characteristic is soft due to plasticity. However, the formation of zones of ambiguity is hampered by the high level of internal energy dissipation.

Since aluminum alloys have very low cyclic hardening, the frequency characteristic for stresses has a plateau in the plastic domain.

An analysis reveals that the standard model is in good agreement with the exact (numerical) solution in kinematic characteristics—total and plastic strains. However, it strongly overestimates the stresses.

Denote by f^* the frequency at which the strain amplitude peaks at a fixed amplitude of excitation. In particular, for $e_0^* = 0.1\cdot 10^{-2}$ and $0.2\cdot 10^{-2}$ we have $f_1^* = 223$ Hz and $f_2^* = 190$ Hz, respectively. For $f > f^*$, the modified model is also in good agreement with the exact solution. It produces a lower bound for strains, and the standard model an upper bound. For $f < f^*$, the modified model overestimates the inelastic strains.

Thus, to obtain exacter estimates for both strain and stress characteristics, it is worthwhile to carry out double evaluation of plastic systems using both linearization schemes.

An analysis shows that an increasing load s_0 leads to disturbance of the mainly monoharmonic vibration process because of increased contribution of subharmonics. In this case, the potentialities of the approximate schemes are exhausted; and reliable information can be drawn with the help of direct numerical integration of the problem.

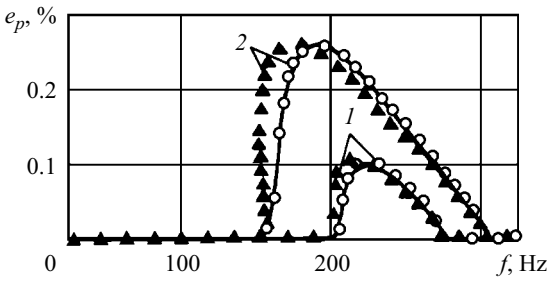

Fig. 8.3

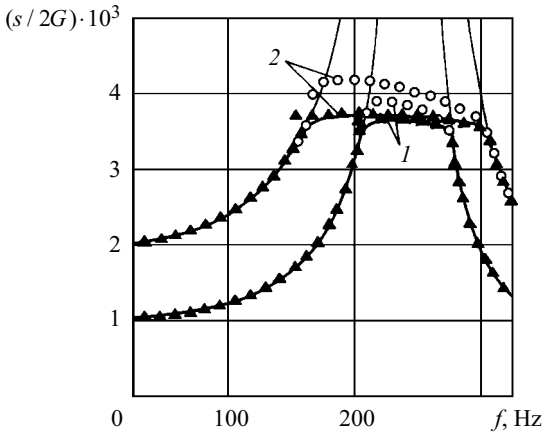

Fig. 8.4

9. Complete Formulation of the Thermomechanic Problem for Physically Nonlinear Bodies. The thermodynamics of the Bodner–Partom model was developed in [7, 45, 46, 71]. The resulting constitutive equations for entropy and dissipation rates provide a basis for formulating the thermomechanic problem in [18–20, 22, 44, 49]. It includes:

the representation of the total strain as the sum of elastic, inelastic, and thermal components

$$\boldsymbol{\epsilon} = \boldsymbol{\epsilon}^e + \boldsymbol{\epsilon}^p + \boldsymbol{\epsilon}^\theta, \tag{9.1}$$

the Cauchy relations

$$\varepsilon = \frac{1}{2}\left[\nabla\vec{u} + (\nabla\vec{u})^T\right], \tag{9.2}$$

the expression for thermal strain

$$\boldsymbol{\epsilon}^\theta = \boldsymbol{I}\int_{\theta_0}^{\theta} \alpha(\theta')\, d\theta', \tag{9.3}$$

Hooke's law for elastic strain

$$\boldsymbol{s} = 2G\left(\boldsymbol{e} - \boldsymbol{\epsilon}^p\right), \qquad \operatorname{tr}\boldsymbol{\sigma} = 3K_V \operatorname{tr}\left(\boldsymbol{\epsilon} - \boldsymbol{\epsilon}^\theta\right), \tag{9.4}$$

the flow equation

$$\dot{\boldsymbol{\epsilon}}^p = \frac{D_0}{\sqrt{J_2}} \exp\left[-\frac{1}{2}\left(\frac{Z}{\sqrt{3J_2}}\right)^{2n}\right]\boldsymbol{s}, \qquad \boldsymbol{\epsilon}^p(0) = 0, \tag{9.5}$$

the complete evolution equations of isotropic and kinematic hardening

$$\dot{K} = m_1\left(K_1 - K\right)\dot{W}_p - A_K K_1\left[\left(K - K_2\right)/K_1\right]^{r_K}, \qquad K(0) = K_0, \tag{9.6}$$

$$\dot{\boldsymbol{\beta}} = m_2\left(D_1\boldsymbol{u} - \boldsymbol{\beta}\right)\dot{W}_p - A_D K_1\left[(\boldsymbol{\beta}:\boldsymbol{\beta})^{1/2}/K_1\right]^{r_D}\boldsymbol{V}, \qquad \boldsymbol{\beta}(0) = 0, \tag{9.7}$$

the equation of motion

$$\operatorname{div}\boldsymbol{\sigma} - \rho\ddot{\vec{u}} = 0, \tag{9.8}$$

the nonstationary heat conduction equation (energy equation)

$$c_V\dot{\theta}+3\alpha_0\theta K_V\left(\operatorname{tr}\dot{\boldsymbol{\epsilon}}-3\alpha_0\dot{\theta}\right)-D'-k\Delta\theta=r, \tag{9.9}$$

the expression for the dissipation rate

$$D'=\boldsymbol{\sigma}\cdot\dot{\boldsymbol{\epsilon}}^p-\boldsymbol{\beta}\cdot\dot{\boldsymbol{\alpha}}-K\dot{\delta}, \tag{9.10}$$

where $Z=K+D$, $J_2=\boldsymbol{s}\cdot\boldsymbol{s}/2$, $\dot{W}^p=\boldsymbol{\sigma}\cdot\dot{\boldsymbol{\epsilon}}^p$, $\boldsymbol{u}=\boldsymbol{s}/(\boldsymbol{s}\cdot\boldsymbol{s})^{1/2}$, $\boldsymbol{V}=\boldsymbol{\beta}/(\boldsymbol{\beta}\cdot\boldsymbol{\beta})^{1/2}$, $D=\boldsymbol{\beta}\cdot\boldsymbol{u}$, $\vec{u}$ is the displacement vector; G and K_V are the shear and bulk moduli; and c_V, α_0, and k are the coefficients of thermal capacity, linear thermal expansion at reference temperature $\theta=\theta_0$, and thermal conductivity, respectively.

According to [58, 69], D_0, D_1, K_1, m_1, m_2, r_K, and r_D are temperature-independent coefficients; n, K_0, K_2, A_K, A_D, K_V, and G are functions of temperature; and δ and $\boldsymbol{\alpha}$ are the thermodynamic displacements conjugate to the thermodynamic forces K and $\boldsymbol{\beta}$, respectively. The evolution equations determining them are given in [7, 45].

Boundary and initial conditions close the formulation of the problem.

10. Approximate Formulation of the Thermomechanics Problem for Physically Nonlinear Bodies. Based on the MHA schemes proposed in Section 2 and 3, the authors of [44, 49] propose an approximate formulation of the thermomechanic problem for physically nonlinear bodies. The corresponding formulas are presented below:

$$\tilde{\boldsymbol{s}}=2\tilde{G}\tilde{\boldsymbol{e}},\qquad \tilde{\boldsymbol{\epsilon}}^p=\tilde{\lambda}\tilde{\boldsymbol{e}}, \tag{10.1}$$

$$\tilde{\boldsymbol{e}}=\boldsymbol{e}'+i\boldsymbol{e}'',\qquad \tilde{\boldsymbol{s}}=\boldsymbol{s}'+i\boldsymbol{s}'',\qquad \tilde{\boldsymbol{\epsilon}}^p=\boldsymbol{\epsilon}'+i\boldsymbol{\epsilon}'', \tag{10.2}$$

$$\tilde{G}=G'+iG'',\qquad \tilde{\lambda}=\lambda'+i\lambda'', \tag{10.3}$$

where $\tilde{\boldsymbol{e}}$, $\tilde{\boldsymbol{s}}$, and $\tilde{\boldsymbol{e}}^p$ are the complex amplitudes of the deviators of total strain, stress, and plastic strain; $\tilde{G}_N$ and $\tilde{\lambda}_N$ are the complex shear modulus and inelasticity coefficient, respectively; and the real and imaginary parts of complex quantities are denoted by $(\cdot)'$ and $(\cdot)''$, respectively.

The moduli $\tilde{G}$ and $\tilde{\lambda}$ are functions of the intensity of strain amplitude tensor e_i^2, frequency ω, and, in the general case, temperature θ:

$$\tilde{G}=\tilde{G}\left(e_i,\omega,\theta\right),\qquad \tilde{\lambda}=\tilde{\lambda}\left(e_i,\omega,\theta\right),$$

where $e_i^2=\boldsymbol{e}'\cdot\boldsymbol{e}'+\boldsymbol{e}''\cdot\boldsymbol{e}''$.

The real and imaginary parts of the complex moduli are determined by formulas (3.6) and (3.7) using cyclic diagrams calculated by direct numerical integration of the Bodner–Partom equations for uniaxial tension or shear.

Note that, in the general case, the approximate model can be completely specified based on experimental cyclic diagrams. The Bodner–Partom model is used here to estimate the accuracy of the approximate approach

The equations of the simplified model (10.1)–(10.3) are supplemented with the complex analog of the vibration equation

$$\operatorname{div}\tilde{\boldsymbol{\sigma}}+\rho\omega^2\tilde{\vec{u}}=0. \tag{10.4}$$

The approximate formulation of the thermoviscoplastic problem includes the period-average heat-conduction equation that has the following form if the thermoelastic effects are neglected, $3\alpha K_V\langle\theta\operatorname{tr}\dot{\boldsymbol{\epsilon}}\rangle\approx 0$ and $9\alpha\theta K_V/c_V\approx 0$:

$$c_V\dot{\bar{\theta}}-k\Delta\bar{\theta}-\langle D'\rangle_N=0, \tag{10.5}$$

where $\bar{\theta}$ is the period-average temperature.

Similarly, averaging the expression for the dissipation rate and neglecting the effect of "cold" work, we obtain

$$\langle D'\rangle=\langle\dot{W}_p\rangle=\langle\boldsymbol{s}\cdot\dot{\boldsymbol{e}}\rangle. \tag{10.6}$$

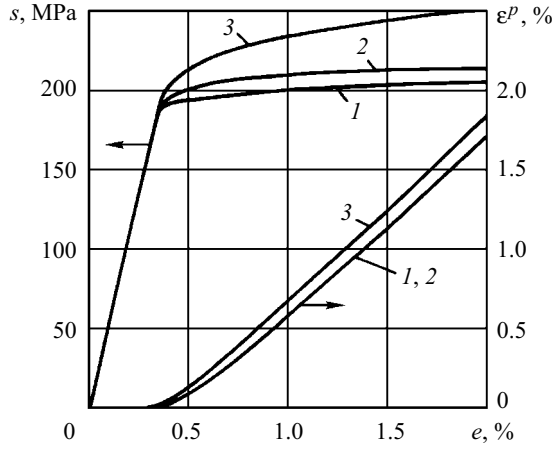

Fig. 11.1

The system of equations (10.1)–(10.6) is supplemented with complex analogs of the boundary and initial (for temperature) conditions.

11. Resonant Vibrations and Dissipative Heating of a Homogeneous Disk. The authors of [19, 20, 22] used the exact and approximate formulations of thermomechanic problems for physically nonlinear materials (Sections 9 and 10) to study the resonant vibrations and dissipative heating of a homogeneous disk $|z| \le H$, $0 < r < R$, made of AMg-6 aluminum alloy.

The complex characteristics $\widetilde{G}$ and $\widetilde{\lambda}$ of the approximate model were determined, by the second approach, from the cyclic diagrams $s(e_0, \omega)$ and $\varepsilon^p(e_i, \omega)$ for the strain cycle and $s(s_i, \omega)$ and $\varepsilon^p(s_i, \omega)$ for the stress cycle, since these diagrams can differ depending on whether the cycle is strain- or stress-controlled. To this end, the Bodner–Partom equations were numerically integrated for the case of a thin-walled cylinder under cyclic torsion. These diagrams and the dissipation characteristics found were used to calculate, by formulas (3.6) and (3.7), the real and imaginary parts of the complex moduli, which are needed to solve problems in approximate formulation.

The cyclic diagrams for AMg-6 alloy at $f = 230$ Hz are shown in Fig. 11.1. Curves *1* and *2* correspond to the modified approach (strain (hard) and stress (soft) cycles, respectively), and curves *3* correspond to the standard approach (strain cycle). As is seen, the curves for strain- and stress-controlled cycles of loading differ insignificantly, which confirms the adequacy of the well-known Serensen–Gusenkov–Makhutov hypothesis.

The values of G'/G and G''/G calculated by the modified scheme at $f = 230$ Hz for a cyclic steady-state deformation process are presented in Table 1. The loading conditions at the lateral surface $r = R$ of the disk can be written in exact and approximate formulations as follows:

$$\sigma_{rr} = -\sigma_0 \frac{z}{H} \sin \omega t, \quad \sigma_{rz} = 0, \qquad \widetilde{\sigma}_{rr} = -i\sigma_0 \frac{z}{H}, \quad \sigma_{rz} = 0, \tag{11.1}$$

where σ_0 is the load parameter.

The methods of numerical solution of the problem in exact, (9.1)–(9.10), and approximate, (10.1)–(10.6), formulations are similar to the approaches developed in [18–20, 22, 56].

The disk is characterized by the following geometrical parameters: $H = 0.2 \cdot 10^{-2}$ m, $R = 0.2$ m. The first resonant frequency of the disk is $f_r = 246$ Hz; it corresponds to the first bending mode. The ambient temperature and the heat-transfer factor are $\theta_c = 20$ °C, $\alpha = 30$ W/m^2 °C.

The objective of the analysis is to evaluate the capabilities of the approximate approach to solve axisymmetric dynamic thermoviscoplastic problems.

The exact and approximate models are compared by the following characteristics: intensities of amplitudes of total shear strains e_i, inelastic strains e_i^p, tangential stresses s_i, period-average dissipation rate $\overline{D}'$, maximum stored energy W, and volume-average values $\langle \overline{D}' \rangle_V$ and $\langle W \rangle$ of $\overline{D}'$ and W. The exact and approximate expressions for these characteristics are given in

TABLE 1

e_i, %	G'/G	G''/G
0.0	1.0	0.0
0.20	1.0	0.0
0.25	1.0	0.0
0.30	0.942	0.139
0.35	0.824	0.245
0.40	0.717	0.298
0.60	0.438	0.330
0.70	0.358	0.316
0.80	0.300	0.298
0.90	0.255	0.280
1.00	0.221	0.263
1.20	0.171	0.234
1.40	0.138	0.209
1.60	0.114	0.189
1.80	0.096	0.172

TABLE 2

Exact formulation	Approximate formulation
$e_i = \left[\frac{1}{8}\Delta e_{ij}\Delta e_{ij}\right]^{1/2},$ $e_i^p = \left[\frac{1}{8}\Delta e_{ij}^p \Delta e_{ij}^p\right]^{1/2},$ $s_i = \left[\frac{1}{8}\Delta s_{ij}\Delta s_{ij}\right]^{1/2},$ $\overline{D}' = \frac{1}{T}\int_0^T \sigma_{ij}\dot{e}_{ij}^p dt,$ $\langle \overline{D}' \rangle_V = \frac{1}{V}\int_V \overline{D}' dv,$ $W = \max_T\left[\frac{\sigma_{kk}^2}{18K_V} + \frac{s_{ij}s_{ij}}{4G}\right],$ $\langle W \rangle_V = \frac{1}{V}\int_V W dv.$	$e_i = \left[\frac{1}{2}\left(\tilde{e}_{ij}\tilde{e}_{ij}^*\right)\right]^{1/2},$ $e_i^p = \left[\frac{1}{2}\left(\tilde{e}_{ij}^p\tilde{e}_{ij}^{p*}\right)\right]^{1/2},$ $s_i = \left[\frac{1}{2}\tilde{s}_{ij}\tilde{s}_{ij}^*\right]^{1/2},$ $\overline{D}' = \frac{\omega}{2}\operatorname{Im}\left(\tilde{s}_{ij}\tilde{e}_{ij}^*\right),$ $\langle \overline{D}' \rangle_V = \frac{1}{V}\int_V \overline{D}' dv,$ $W = \left[\frac{\tilde{\sigma}_{kk}\tilde{\sigma}_{kk}^*}{18K_V} + \frac{\tilde{s}_{ij}\tilde{s}_{ij}^*}{4G}\right],$ $\langle W \rangle_V = \frac{1}{V}\int_V W dv.$

TABLE 3

Model	s_i, MPa	e_i, %	e_i^p, %	$\overline{D}'$, MW/m^3	$\langle \overline{D}' \rangle_V$, MW/m^3	W, MJ/m^2	$\langle W \rangle_V$, MJ/m^2	$\Delta u_z \cdot 10$, m
1	201.9	0.876	0.576	2072.0	44.6	0.982	0.200	0.188
2	235.1	0.840	0.535	1964.0	46.9	1.342	0.242	0.193
3	200.2	0.926	0.621	2290.0	44.6	0.973	0.204	0.184
4	208.3	0.911	0.601	2293.0	45.3	1.050	0.212	0.186
5	207.0	0.726	0.508	1916.0	37.8	1.040	0.181	0.160

Table 2, $\tilde{a}^* = a' - ia''$, $\Delta(\cdot) = \max_T(\cdot)(t) - \min_T(\cdot)(t)$. All the characteristics, except for those averaged over the volume, have been calculated at the point $r = 0$, $z = H$ for f = 230 Hz and $\sigma_0 = 50$ MPa.

The calculated results are presented in Table 3: exact results in row 1; approximate results based on cyclic diagrams 1–3 (Fig. 11.1) in rows 2–4, respectively; and results obtained by the standard model for stress-controlled cycle of loading in row 5. The range of axial displacement Δu_z is also calculated at the point $r = 0$, $z = H$.

For convenience of comparative analysis, we will identify the approximate models with row numbers in Table 3.

By and large, all approximate models demonstrate very high accuracy of calculating the maximum stress/strain characteristics and integral energy characteristics. All the models, except for model 3, overestimate the intensity of plastic strain. From this point of view, model 3 is preferable for low-cycle fatigue based on the Coffin–Manson criterion. This same model

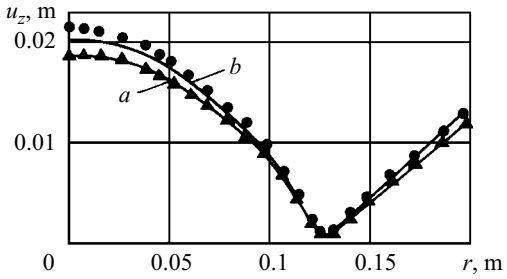

Fig. 11.2

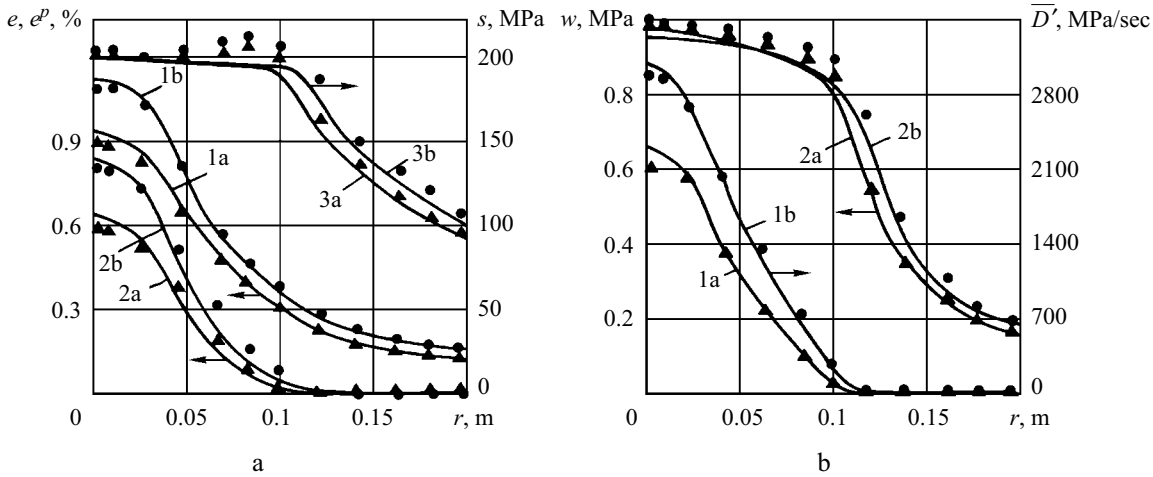

Fig. 11.3

gives the best estimates for volume-average dissipation, stored energy, and displacements. Therefore, this model, which corresponds to the modified scheme with strain-controlled cyclic loading, will be used below to compare the exact and approximate approaches.

The spatial distributions of field quantities are compared in the section $z = H$ of the disk (Figs. 11.2 and 11.3). The triangles and circles stand for the exact amplitudes of loads $\sigma_0 = 50$ MPa and $\sigma_0 = 75$ MPa; and solid lines *a* and *b* represent the approximate solutions for the same loads.

Figure 11.2 shows the vibration mode of the disk. The maximum transverse displacements are observed at the middle of the disk. Despite the presence of large inelastic strains, the radial distribution of displacements is nearly elastic. The results produced by the exact and approximate models are in good agreement.

Figure 11.3a shows the intensities e_i, e_i^p, and s_i (curves *1–3*, respectively); and Fig. 11.3b shows the distributions of $\overline{D}'$ and W (curves *1* and *2*, respectively) obtained in solving the problem in approximate formulation. As is seen, the approximate and exact results are in good agreement. Both models predict the formation of a zone of inelastic deformation at the middle of the disk and elastic deformation of its boundary zones. As a result, the stress distribution has a plateau at the middle with values close to the cyclic yield point. The distribution of the maximum stored energy W has a similar form.

Figure 11.4 shows the amplitude–frequency characteristics for the deflection u_z (curve *1*), the intensity of tangential stresses s_i (curve *2*), inelastic strains e_i^p (curve *5*), and temperatures θ (curve *4*). Curve *1* refers to the left-hand axis, and curves *2–4* to the right-hand axis. The thin lines represent linearly elastic characteristics. Comparing the curves, we identify the main viscoplastic effects: finite resonant amplitudes, soft characteristics, plateau-like frequency dependence of stress intensity, and inelastic strains and dissipative heating in a finite frequency range.

12. Resonant Vibrations and Dissipative Heating of a Laminated Disk [99]. To evaluate the capabilities of the MHA model as applied to piecewise-homogeneous bodies, let us turn to the flexural vibrations and dissipative heating of a three-layer disk $|z| \le H$, $0 \le r \le R$, excited at its edges by a harmonic axisymmetric load. The middle layer $|z| \le h_1$ and face layers $h_1 \le |z| \le H$ are made of dissimilar viscoplastic materials and are in perfect thermal and mechanical contact.

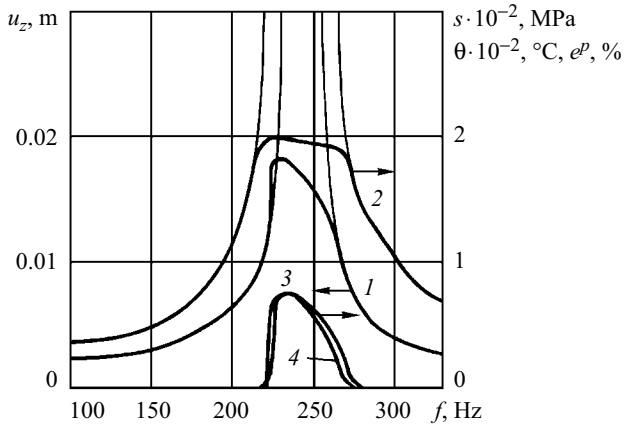

Fig. 11.4

TABLE 4

Model	s_i, MPa	e_i, %	e_i^p, %	$\overline{D}'$, MW/m^3	$\langle \overline{D}' \rangle_V$, MW/m^3	W, MJ/m^2	$\langle W \rangle_V$, MJ/m^2	$\Delta u_z \cdot 10$, m
Exact	203.4	0.875	0.575	2276.0	61.9	1.048	0.284	0.141
Approximate	199.7	0.898	0.599	2348.7	57.4	0.967	0.259	0.147

The geometrical parameters of the three-layer disk are: R = 0.175 m, $H = 0.2 \cdot 10^{-2}$ m, $h_1 = 0.1 \cdot 10^{-2}$ m. The resonance frequency of the disk in the first axisymmetric bending mode is f_r = 248 Hz. The excitation frequency f is also equal to 248 Hz. The temperature θ_0 is equal to 20 °C. The domain of interest was partitioned into a fine finite-element mesh. A typical mesh contains 140 quadrangles and 469 nodal points.

Figure 12.1 allows us to assess the accuracy of the approximate model. The circles and triangles stand for the nodal intensity of stresses and inelastic strains calculated by the exact model for σ_0 = 70 MPa. It is seen that the amplitudes of intensities of stresses and inelastic strains calculated by the exact model fit well the diagrams $s_i(e_i)$ and $e_i^p(e_i)$ obtained by the approximate model for a strain cycle.

The exact and approximate results are compared by the same characteristics as in Section 11 (Table 2). All the characteristics, except for those averaged over the volume, are calculated at the point $r = 0$, $z = H$ for f = 248 Hz and σ_0 = 70 MPa.

The results are presented in Table 4. The first and second rows contain the exact and approximate solutions, respectively. The data are in good agreement.

The radial distributions of field quantities are compared in the section $z = H$ (Fig. 12.2) and the thickness distributions at the disk center, r = 0 (Fig. 12.3). The solid lines represent the approximate results and the symbols stand for the exact solution. Lines *1* and the diamonds refer to the displacement ranges u_z; lines *2* and the open squares to the intensities of amplitudes of total strain deviators e_i; lines *3* and the full squares to the intensities of amplitudes of inelastic strain e_i^p; lines *4* and the triangles to the intensities of amplitudes of stress deviators s_i; curve *5* and the open circles to the period-average dissipation rate $\overline{D}'$, and lines *6* and the full circles to the temperature increment $\theta - \theta_0$.

An analysis of Fig. 12.2 reveals that the distributions of field quantities are determined by a vibration mode characteristic of the resonance in the first axisymmetric bending mode, for which the maximum displacements and total and inelastic strains are observed at the middle of the disk. The radial distribution of displacements is nearly elastic, despite large inelastic strains. At the middle of the disk, the stress distribution has a plateau with a stress level close to the cyclic yield point. The exact and approximate solutions and also the solution for a homogeneous disk are in good agreement [19, 22].

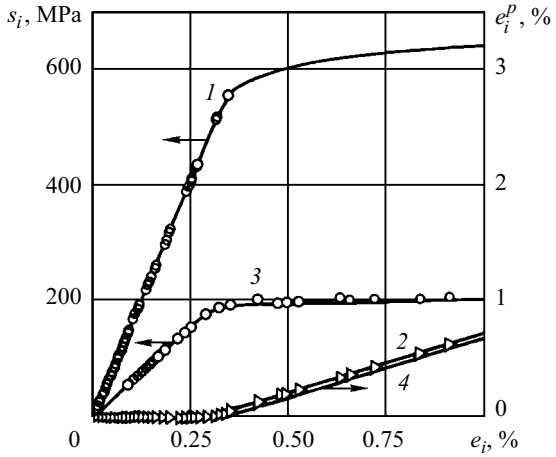

Fig. 12.1

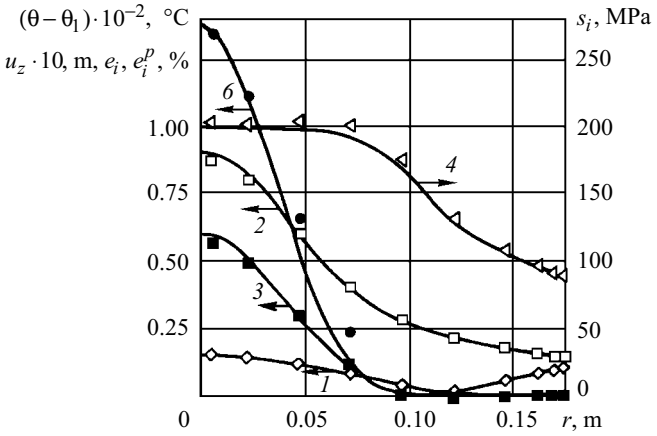

Fig. 12.2

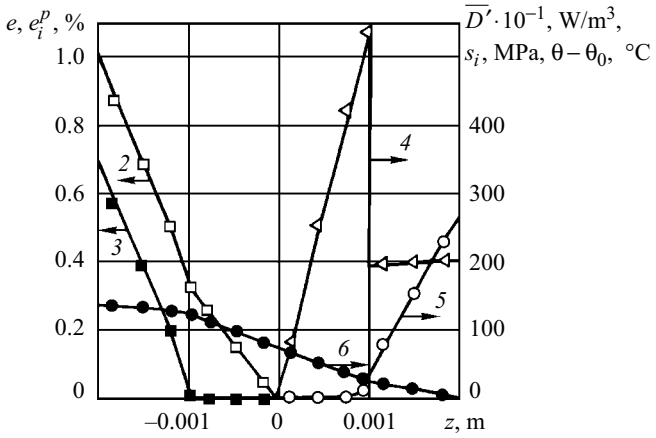

Fig. 12.3

The nonuniformity of the stress–strain state is illustrated in Fig. 12.3. Since the fields are symmetric about the median surface, only half the distribution is shown: e_i and e_i^p for negative values of z, and s_i and $\overline{D}'$ for positive. The thickness distribution of temperature is asymmetric for the chosen boundary conditions and is shown completely.

In contrast to the deformation characteristics, the intensity of stresses is characterized by a discontinuity at the interface. However, this discontinuity in the distribution $\overline{D}'$ is much weaker because of the high uniformity of deformation distributions. As in Fig. 12.2, the exact and approximate data are in good agreement.

Figure 12.4 shows the amplitude–frequency characteristics for u_z, e_i, e_i^p, s_i, and $\overline{D}'$ and also the temperature–frequency characteristic. The curves are numbered as in Figs. 12.2 and 12.3. The thin lines represent linearly elastic characteristics. The quadrangles stand for the exact values of the above-mentioned quantities at the frequency of linear resonance. These data are in good agreement with the approximate results.

The amplitude–frequency characteristics have the following features determined by the viscoplastic behavior of the disk: finite resonant amplitudes, soft nonlinearity, and strong frequency dependence of stress intensity. Moreover, plastic deformation and, consequently, vibrational heating occur within a finite range of frequencies near resonance.

The conclusion that the exact and approximate results are in good agreement is supported by the solutions of plane and axisymmetric problems [6, 8, 12, 21, 47, 48, 96–98].

Thus, the above formulations can be used in low-cycle fatigue analysis of structural members by introducing either Coffin–Manson-type criteria or the evolution equations for damage parameters.

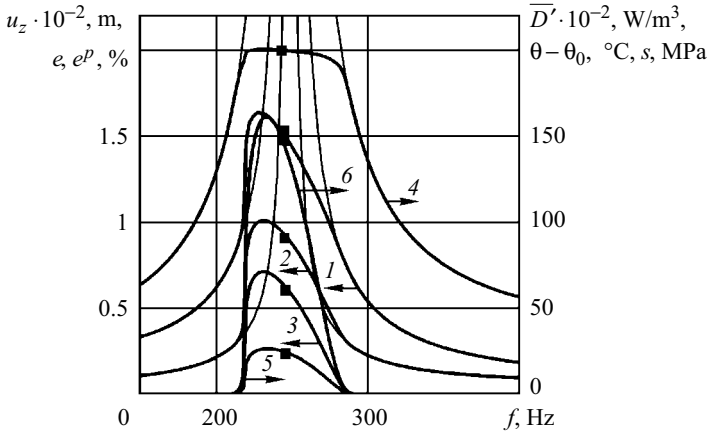

Fig. 12.4

13. Generalized Approximate Model of Microplastic, Macroinelastic Behavior. The authors of [15] proposed a generalized model that allows us, based on the concept of complex moduli, to uniquely describe the cyclic properties of the material in both microplastic and macroinelastic domains.

The amplitude dependence of complex characteristics can be specified in two ways: (i) based on experimental results from studies of dynamic properties in the microplastic and macroinelastic domains and (ii) based on the general relations of multimodal viscoplasticity [7, 46], with one or several lower modes corresponding to microplastic deformation and higher modes to macroinelastic deformation.

To specify these characteristics for the case of microplasticity, we can use the experimental data from [27, 29] on the dependence of the loss angle and absorption factor on load. In processing the data obtained from tension–compression experiments, it is assumed that the bulk modulus K_V is a real constant. In this case, Poisson's ratio is a complex characteristic ($\nu = \tilde{\nu} = \nu' - i\nu''$).

Figure 13.1 demonstrate the generalized shear characteristics for two materials: 12KhN3A steel (curve *1*) and AMg-6 aluminum alloy (curve *2*) for frequency f = 250 Hz. In the figure, the curves of $G'(e_i)$ and $G''(e_i)$ for microplastic (dashed lines) and macroinelastic (solid lines) domains are joined near the cyclic yield point $e_i = e_{iT} \approx 0.3\%$. As a result, the generalized dependences $G'(e_i)$ and $G''(e_i)$ are represented by curves *1a* and *1b*, consisting of dashed and solid sections, for steel and by similar curves *2a* and *2b* for aluminum alloy. Dash-and-dot curves *2b* and *1b* corresponding to macrolosses in the transition domain are replaced with higher microplastic damping.

The curves of G' practically coincide (to within graphical accuracy) with the curves plotted regardless of microplasticity. The curves of G'' differ essentially. In the macroinelastic case, $G'' \equiv 0$ for $e_i < e_{iT}$. In the generalized model, $G'' \neq 0$ in the same domain because of microplastic intrinsic losses.

Though the transition domain is, apparently, of complex structure and has not been studied well enough, the piecewise approximation of the amplitude dependence of the characteristics is used for simplicity (Fig. 13.1). Their common feature is abrupt increase in intrinsic losses for $e_i > e_{iT}$.

The capabilities of the model are illustrated by an example of flexural vibrations of a three-layer beam ($0 \le x \le L$, $|z| < H_s / 2$, where H_s is the total thickness ($H_s = h_1 + h_2 + h_3$, where h_1, h_2, and h_3 are the layer thicknesses)). Here $L = 0.76$ m, $H_s = h_y = 0.3 \cdot 10^{-1}$ m, $h_1 = h_3 = 0.3 \cdot 10^{-2}$ m, and $h_2 = 0.24 \cdot 10^{-1}$ m.

Vibrations are excited by moments applied at the ends $x = 0, L$,

$$M_x = -\frac{\sigma_{xx}^0 H_s^2}{6} \sin \omega t = -M_0 \sin \omega t,$$

where σ_{xx}^0 is the load parameter.

The middle layer of the beam is made of steel, and the face layers of aluminum alloy. Their characteristics are represented in Fig. 13.1. The frequency of the first symmetric linearly elastic resonance of the beam is f_{r1} = 252 Hz.

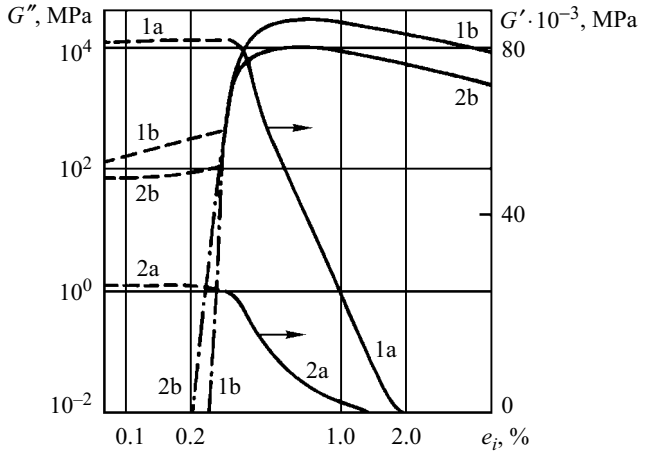

Fig. 13.1

Figure 13.2 shows the resonant amplitude–frequency characteristics for the intensity of shear stresses at the point $x = 0.38$ m, $z = 0.15 \cdot 10^{-1}$ m (the point of maximum intensity in the AMg-6 layer) for different values (in MPa) of σ_{xx}^0.

The authors of [15] introduced the concept of conditional critical load, which determines microplastic–macroinelastic transition. It is a load $\sigma_{xx}^0 = \sigma_T^*$ under which the intensity of amplitudes of inelastic strains reaches a level determined by some tolerance. It is equal to 0.2%, by analogy with the technical theory of plasticity.

This quantity can be used to evaluate fatigue strength and thermal state in the domain of transition from high-cycle to low-cycle fatigue.

It was established that the critical load for the aluminum layer corresponding to the tolerance for the intensity of macroinelastic strains is $\sigma_T^* = 1.5$ MPa. Thus, the curve for $\sigma_{xx}^0 = 1.0$ MPa still refers to the microplastic domain. For $\sigma_{xx}^0 > \sigma_T^*$, macroinelasticity becomes the dominant nonlinear factor. Therefore, at the resonant frequency, the curves for $\sigma_{xx}^0 = 2.5$, 10, 50 MPa have a plateau-like form, typical for plastic materials, with $s_i^{\max} \approx s_T$, where s_T is the cyclic limit of inelasticity in torsion.

Each layer can be characterized by an individual critical load σ_{TN}^*, where N is the layer number. However, they appear practically equal because of the small thickness of external layers and close deformation limits of inelasticity. For other geometry and other materials, the critical loads may be different.

Let us consider the damping characteristics of a beam with microplastic losses taken into account. Figure 13.3 demonstrates how the level of loading of the three-layer beam affects the maximum stationary redundant temperature of vibrational heating for two excitation frequencies: $f = 252$ Hz (curve *1*) and $f = 1$ Hz (curve *2*). As expected, the levels of heating are equal at resonance under lower levels of loading than those in the case of quasistatic vibrations. However, in the latter case, the heating temperature increases abruptly after the critical load is exceeded, by analogy with the absorption factor.

14. Cyclic Deformation of Bodies with Stress Concentrators. The exact and approximate analyses of bodies with stress concentrators, in particular internal defects are compared in [9, 11, 13, 50, 90]. It was established that the stress and strain concentration factors calculated using the exact and approximate models are in good agreement.

The authors of the cited publications assessed reversible and irreversible temperature effects at internal and surface concentrators in inelastic bodies and discussed the possibilities of using them to identify damages.

An unexpected result was that there is no local vibrational heating near the cut despite the high level of stress/strain concentration. This is due to the high thermal diffusivity of metals. Recent studies indicate that the effects of local heating are better manifested in polymeric bodies [59, 74]. A theoretical analysis reveals that such effects also occur in metal bodies at ultrasonic frequencies of loading.

15. Thin-Walled Elements. The physical MHA equations mentioned above were used in [10, 23, 24, 96] to construct an approximate dynamic thermomechanical model of thin-walled elements, based on the Kirchhoff–Love hypotheses.

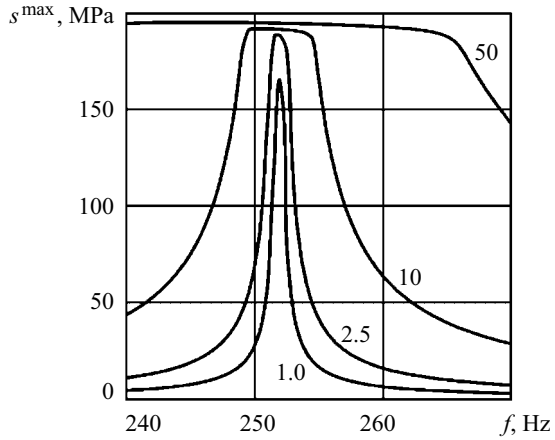

Fig. 13.2

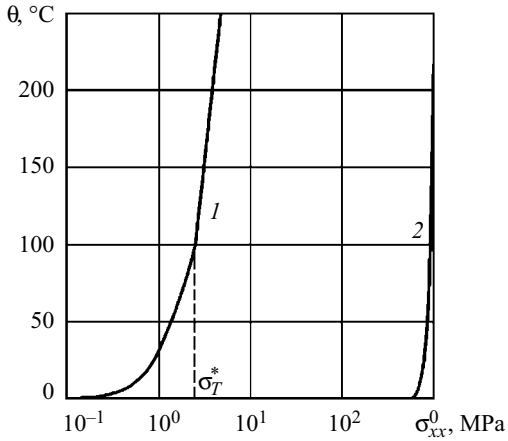

Fig. 13.3

It turned out that both local and integral stress/strain and thermal characteristics obtained by the exact and approximate models are in good agreement.

Recently much attention has been given to new principles of controlling the vibrations of structural members, in particular thin-walled members [95]. The authors of [16, 17] generalized the results mentioned above to thin-walled members containing both passive metal layers and active piezoelectric layers. The paper [14] substantiated a linear control law of electric potential with a complex control factor that allows suppressing completely the resonant vibration of the beam. In this case, dissipative heating is not due to the dissipation of mechanical energy but rather due to the dielectric losses in piezoactive layers.

16. Allowing for Damageability. An important effect that accompanies cyclic deformation and characterizes the state of the material is damage [87].

Damage incorporated into the constitutive equations considered above increases the rates of both elastic and inelastic strains; though the latter is more important for plastic metals. In the generalized flow models, the isotropic damage parameter Ω, $0 \le \Omega \le 1$, is introduced into the flow equation (9.5) as a softening parameter that decreases resistance to inelastic deformation. This is done by replacing the hardening parameter Z in Eq. (9.5) by $Z(1-\Omega)$ [69]. According to [86], the critical level of damage causing failure of metals ranges from 0.15 to 0.85.

Bodner and Chen [70] proposed the following equation for isotropic damage under multiaxis stress:

$$\dot{\Omega} = \frac{p}{H}\left(\ln\frac{1}{\Omega}\right)^{\frac{p+1}{p}} \Omega\dot{Q}, \qquad \Omega(0) \approx 0, \tag{16.1}$$

where the generalized stress $\dot{Q}$ is defined [80] by

$$\dot{Q} = \left(A\sigma_1^{+} + B\sigma_{eff} + CI_1\right)^z, \tag{16.2}$$

where σ_1^{+} is the maximum principal tensile stress; $\sigma_{\text{eff}} = (3J_2)^{1/2}$; I_1 is the first invariant of the stress tensor; and p, H, A, B, C, and z are material constants, $A + B + C = 1$.

The authors of [70] demonstrated that the replacement $Z \to Z(1-\Omega)$ in combination with Eqs. (16.1) and (16.2) provides good fit to experimental data.

In monoharmonic approximation, damage is allowed for by including the parameter Ω in the set of arguments of the complex shear modulus. For some materials such as rock, a similar dependence can also be considered for the bulk modulus. For proportional loading, we obtain

$$\widetilde{G} = \widetilde{G}(\omega, \theta, e, \Omega), \qquad K_V = K_V(\theta, \Omega). \tag{16.3}$$

Equation (16.1) remains the same. However, the parameter Ω is regarded as averaged over the period of vibrations, $\Omega \to \langle\Omega\rangle$.

The effective stress in (16.2) may be replaced by its amplitude analog:

$$\dot{Q} = \left(A\sigma_1^{\dagger} + Bs_i + CI_1 \right)^z . \tag{16.4}$$

17. Disproportionate Cyclic Loading. Extensive experimental data show that the dependence of material functions only on the intensity of strain or stress adequately describes the behavior of materials that are subject to proportional (simple) loading. Models of inelasticity are generalized to the case of disproportionate loading by introducing new parameters and complicating the flow rule. In particular, the flow rule (9.5) in the Bodner–Partom model is modified as follows [69]:

$$\dot{\varepsilon}_{ij}^{\,p} = \lambda s_{ij} + g(\lambda) F n_{ij} , \tag{17.1}$$

where n_{ij} is a tensor normal to the stress deviator s_{ij}; F is a dimensionless function of hardening parameters; and $g(\lambda)$ is the Heaviside function that is equal to 1 in the inelastic domain.

The tensor n_{ij} is a deviator and is expressed in terms of the components of the deviator of total strain rate

$$n_{ij} = \dot{e}_{ij} - \left(\dot{e}_{kl} \cdot u'_{kl} \right) u'_{ij} , \tag{17.2}$$

where u'_{ij} determines the direction of the tensor s_{ij}, $u'_{ij} = s_{ij} / |s_{ij}|$.

The tensor n_{ij} is nonzero only in the case of disproportionate loading.

Success in the approximation of experimental data strongly depends on the choice of additional scalar or tensor measures of disproportionate loading. The possibilities arising here were tested in [68, 72, 76, 84, 85, 93, 94] for various models of plasticity and viscoplasticity. Let us consider, within the framework of the monoharmonic-deformation model, the phase difference between two components of the strain tensor.

Consider the MHA relation (1.4). In the Cartesian coordinate system $Ox_1x_2x_3$ for $\bar{\varepsilon}_{ij} = 0$, we have

$$\varepsilon_{ij}(t) = \left| \tilde{\varepsilon}_{ij} \right| \cos\left(\omega t + \varphi_{ij} \right) , \quad i, j = 1, 2, 3, \tag{17.3}$$

where φ_{ij} are phases, $\cos\varphi_{ij} = \varepsilon'_{ij} / |\tilde{\varepsilon}_{ij}|$, $\sin\varphi_{ij} = \varepsilon''_{ij} / |\tilde{\varepsilon}_{ij}|$.

Selecting the phase φ_{11} of the component ε_{11} as reference and using (17.3) for the phase difference $\psi_{mn} = \varphi_{mn} - \varphi_{11}$ between the components ε_{mn} and ε_{11}, we obtain

$$\sin\psi_{mn} = \frac{2}{\omega} \frac{\langle \dot{\varepsilon}_{mn} \varepsilon_{11} \rangle}{|\tilde{\varepsilon}_{mn}| |\tilde{\varepsilon}_{11}|} = \frac{2}{\omega} \frac{\varepsilon''_{11} \varepsilon'_{mn} - \varepsilon'_{11} \varepsilon''_{mn}}{|\tilde{\varepsilon}_{mn}| |\tilde{\varepsilon}_{11}|} , \quad m, n = 1, 2, 3 .$$

It is obvious that when loading is proportional, i.e., $\varepsilon''_{mn} = \eta \varepsilon'_{mn}$, $\eta = \text{const}$, we have $\sin\psi_{mn} = 0$. If the phase shift is equal to 90°, then $\sin\psi_{mn} = 1$. Five values of $\sin\psi_{mn}$ provide a complete set of phase differences of strain components.

Mechanical considerations suggest that any parameter of disproportion A does not depend on the reference phase φ_{11}, i.e., satisfies the identity $A(\psi_{mn}) \equiv A(\psi_{mn} + \bar{\varphi}_{11})$, where $\bar{\varphi}_{11}$ is an arbitrary perturbation of the reference phase φ_{11}.

The following five difference parameters satisfy this condition:

$$S = \{ \sin\left(\psi_{12} - \psi_{13}\right), \sin\left(\psi_{13} - \psi_{23}\right), \sin\left(\psi_{23} - \psi_{22}\right), \sin\left(\psi_{22} - \psi_{33}\right), \sin\left(\psi_{33} - \psi_{12}\right) \},$$

and

$$\sin\left(\psi_{lk} - \psi_{pq}\right) = \frac{\varepsilon'_{pq} \varepsilon''_{lk} - \varepsilon'_{lk} \varepsilon''_{pq}}{|\tilde{\varepsilon}_{lk}| |\tilde{\varepsilon}_{pq}|} .$$

To generalize the concept of complex moduli to the case of disproportionate loading and to allow for the effect of additional cyclic hardening, an additional set of parameters S are included in the set of arguments of complex moduli: $\tilde{G} = \tilde{G}(\omega, \theta, e_i, S)$. The same set of parameters S can also be introduced into Eqs. (16.1), (16.3), and (16.4) of the damage model to allow for the effects of disproportionate loading on fatigue strength.

REFERENCES

1. N. I. Bezukhov, V. L. Bazhanov, I. I. Gol'denblat, N. A. Nikolaenko, and A. M. Sinyukov, *Analysis of Strength*, *Stability*, *and Vibrations at High Temperatures* [in Russian], Mashinostroenie, Moscow (1965).
2. N. N. Bogolyubov and Yu. A. Mitropol'skii, *Asymptotic Methods in the Theory of Nonlinear Vibrations* [in Russian], Nauka, Moscow (1974).
3. V. N. Chelomei, *Vibrations in Engineering: A Handbook* [in Russian], Mashinostroenie, Moscow (1978).
4. S. S. Volkov, Yu. N. Orlov, and B. Ya. Chernyak, *Ultrasonic Welding of Plastics* [in Russian], Khimiya, Moscow (1974).
5. G. H. James, P. K. Imbrie, and P. S. Hill, "An experimental comparison of several current viscoplastic constitutive models at elevated temperatures," *J. Eng. Mater. Technol*., No. 2, 130–136 (1987).
6. Ya. A. Zhuk, "Scleronomous thermomechanical model of viscoplastic bodies under cyclic loading," in: *Proc. Int. Conf. on Modelling and Investigation of System Stability. Mechanical Systems*, Kiev (1997), p. 56.
7. Ya. A. Zhuk, "Generalizing the thermodynamically consistent isothermal Bodner–Partom model," *Dop. NAN Ukrainy*, No. 5, 60–64 (1999).
8. Ya. A. Zhuk, "Studying the thermoviscoplastic behavior of a three-layer damper under harmonic bending," *Dop. NAN Ukrainy*, No. 3, 44–50 (2000).
9. Ya. A. Zhuk, "Determining the stress/strain concentration factors for viscoplastic bodies under cyclic loading," *Dop. NAN Ukrainy*, No. 6, 49–54 (2000).
10. Ya. A. Zhuk and I. K. Senchenkov, "Dynamic thermoviscoplastic problem for shells of revolution of constant thickness," *Dop. NAN Ukrainy*, No. 6, 52–58 (2001).
11. Ya. A. Zhuk and I. K. Senchenkov, "Concentration of stresses and strains in a notched cylinder of a viscoplastic material under harmonic loading," *Int. Appl. Mech*., **35**, No. 2, 120–127 (1999).
12. Ya. A. Zhuk and I. K. Senchenkov, "The coupled thermomechanical behavior of a three-layer viscoplastic beam under harmonic loading," *Int. Appl. Mech*., **36**, No. 2, 271–279 (2000).
13. Ya. A. Zhuk and I. K. Senchenkov, "Study of the effects of thermomechanical coupling near stress concentrators in viscoelastoplastic bodies," *Int. Appl. Mech*., **37**, No. 1, 85–92 (2001).
14. Ya. A. Zhuk and I. K. Senchenkov, "Modelling the stationary vibrations and dissipative heating of thin-walled inelastic elements with piezoactive layers," *Int. Appl. Mech*., **40**, No. 5, 546–556 (2004).
15. Ya. A. Zhuk and I. K. Senchenkov, "Resonance vibrations and dissipative heating of thin-walled laminated elements made of physically nonlinear materials," *Int. Appl. Mech*., **40**, No. 7, 794–802 (2004).
16. Ya. A. Zhuk and I. K. Senchenkov, "Dynamic thermoviscoplastic relations for thin-walled shells with piezoactive layers," *Teor. Prikl. Mekh*., **34**, 115–121 (2001).
17. Ya. A. Zhuk and I. K. Senchenkov, "Formulation of the dynamic thermoviscoplastic problem for flexible shells with piezoactive layers," *Mekh. Girosk. Sist*., **17**–**18**, 146–154 (2001–2002).
18. Ya. A. Zhuk, I. K. Senchenkov, V. I. Kozlov, and G. A. Tabieva, "Plane dynamic thermomechanical behavior of a viscoplastic beam under cyclic loading," *Dop. NAN Ukrainy*, No. 7, 47–51 (2001).
19. Ya. A. Zhuk, I. K. Senchenkov, V. I. Kozlov, and G. A. Tabieva, "Axisymmetric dynamic thermoviscoplastic problem for bodies of revolution," *Dop. NAN Ukrainy*, No. 3, 58–62 (2002).
20. Ya. A. Zhuk, I. K. Senchenkov, V. I. Kozlov, and G. A. Tabieva, "Axisymmetric dynamic problem of coupled thermoviscoplasticity," *Int. Appl. Mech*., **37**, No. 10, 1311–1317 (2001).
21. Ya. A. Zhuk, I. K. Senchenkov, and G. A. Tabieva, "Vibrations of piecewise-inhomogeneous viscoplastic bodies," *Teor. Prikl. Mekh*., **32**, 49–55 (2001).
22. Ya. A. Zhuk, I. K. Senchenkov, G. A. Tabieva, and O. P. Chervinko, "The complex-moduli solution of an axisymmetric dynamic problem of coupled thermoviscoplasticity under harmonic loading," *Int. Appl. Mech*., **37**, No. 12, 1585–1593 (2001).
23. Ya. A. Zhuk, I. K. Senchenkov, and O. P. Chervinko, "Approximate formulation of the thermoviscoplastic dynamic problem for thin-walled shells of revolution under harmonic loading," *Dop. NAN Ukrainy*, No. 5, 38–44 (2001).
24. Ya. A. Zhuk, I. K. Senchenkov, and O. P. Chervinko, "Formulation of the dynamic thermoviscoplastic problem for flexible shells of revolution," *Dop. NAN Ukrainy*, No. 2, 54–61 (2002).

25. L. M. Kachanov, *Fundamentals of Fracture Mechanics* [in Russian], Nauka, Moscow (1974).
26. R. M. Christensen, *Theory of Viscoelasticity: An Introduction*, Academic Press, New York (1971).
27. V. A. Kuz'menko, *Sound and Ultrasonic Vibrations in Dynamic Testing of Materials* [in Russian], Izd. AN USSR, Kiev (1963).
28. A. Ya. Malkin, A. A. Askadskii, and V. V. Kovriga, *Methods of Measuring the Mechanical Properties of Polymers* [in Russian], Khimiya, Moscow (1978).
29. V. V. Matveev, *Damping of Vibrations of Solids* [in Russian], Naukova Dumka, Kiev (1985).
30. V. V. Matveev and A. P. Zin'kovskii, "Department of Vibrations and Vibration Reliability, Institute for Problems of Strength of the National Academy of Sciences of Ukraine (brief information)," *Vseukr. Nauchn.-Techn. Zh. Vinnits. Gos. Sel./Khoz. Inst*., No. 1, 3–6 (1999).
31. V. V. Moskvitin, *Cyclic Loading of Structural Members* [in Russian], Nauka, Moscow (1981).
32. I. Narisawa, *Strength of Polymeric Materials* [Russian translation], Khimiya, Moscow (1987).
33. N. Ohno and M. Satra, "Detailed and simplified elasto-plastic analyses of a cyclically notched loaded bar ," *Trans. ASME*, *J. Eng. Mater. Tech*., **109**, 194–202 (1987).
34. V. A. Pal'mov, *Vibration of Elastoplastic Bodies* [in Russian], Nauka, Moscow Moscow (1976).
35. Ya. G. Panovko, *Internal Friction in Vibrations of Elastic Systems* [in Russian], Gos. Izd. Fiz.-Mat. Lit., Moscow (1960).
36. Ya. G. Panovko, "Allowing for hysteresis losses in the applied theory of elastic vibrations," *Zh. Tekhn. Fiz*., **23**, No. 3, 486–497 (1953).
37. G. S. Pisarenko, *Vibration of Mechanical Systems with Imperfect Elasticity* [in Russian], Naukova Dumka, Kiev (1970).
38. B. E. Popov and I. P. Pal'tov, *Approximate Methods for Studying Nonlinear Automatic Systems* [in Russian], Nauka, Moscow (1960).
39. I. K. Senchenkov, "Approximate formulation of the nonlinear thermoviscoelastic problem with harmonic actions," *Prikl. Mekh*., **21**, No. 2, 91–99 (1985).
40. I. K. Senchenkov, "Interpretation of the physical equations for nonlinear media under cyclic deformation," *Prikl. Mekh*., **23**, No. 9, 90–98 (1987).
41. I. K. Senchenkov and Ya. A. Zhuk, "Describing the resonant vibrations and dissipative heating of viscoelastoplastic bodies," *Prikl. Mekh*., **28**, No. 11, 30–38 (1992).
42. I. K. Senchenkov and Ya. A. Zhuk, "Abnormal behavior of elastoplastic and viscoelastic beams under harmonic and impulsive loading," *Prikl. Mekh*., **30**, No. 3, 82–88 (1994).
43. I. K. Senchenkov and Ya. A. Zhuk, "Scleronomic cyclic-deformation model of viscoplastic bodies under harmonic loading," *Dokl. NAN Ukrainy*, No. 12, 83–89 (1996).
44. I. K. Senchenkov and Ya. O. Zhuk, "Scleronomic model of coupled thermoviscoplasticity under harmonic loading," *Dop. NAN Ukrainy*, No. 3, 83–89 (1997).
45. I. K. Senchenkov and Ya. A. Zhuk, "Thermodynamic analysis of one thermoviscoplastic model," *Prikl. Mekh*., **33**, No. 2, 41–48 (1997).
46. I. K. Senchenkov, Ya. A. Zhuk, and G. A. Tabieva, "Thermodynamically consistent modifications of the generalized thermoviscoplastic models," *Prikl. Mekh*., **34**, No. 4, 53–60 (1998).
47. I. K. Senchenkov, Ya. A. Zhuk, G. A. Tabieva, and O. P. Chervinko, "Generalized scleronomic model of harmonic deformation of viscoelastoplastic bodies," *Prikl. Mekh*., **33**, No. 6, 40–48 (1997).
48. I. K. Senchenkov, Ya. A. Zhuk, G. A. Tabieva, and O. P. Chervinko, "Monoharmonic approximation in deformation problems for viscoplastic bodies under harmonic loading," *Prikl. Mekh*., **33**, No. 7, 57–64 (1997).
49. I. K. Senchenkov, Ya. A. Zhuk, G. A. Tabieva, and O. P. Chervinko, "Simplified thermoviscoplastic models for bodies under harmonic loading," *Prikl. Mekh*., **33**, No. 9, 24–33 (1997).
50. I. K. Senchenkov, Ya. A. Zhuk, and O. P. Chervinko, "Thermomechanical coupling effects near defects in inelastic bodies," *Int. Appl. Mech*., **37**, No. 7, 913–920 (2001).
51. I. K. Senchenkov and V.G. Karnaukhov, "Thermomechanical behavior of nonlinearly viscoelastic materials under harmonic loading," *Int. Appl. Mech*., **37**, No. 11, 1400–1432 (2001).
52. I. K. Senchenkov, V. G. Karnaukhov, and V. I. Kozlov, "The theory of constitutive equations of nonlinear thermoviscoelasticity under periodic deformation," *Prikl. Mekh*., **22**, No. 8, 97–104 (1986).

53. I. K. Senchenkov, V. G. Karnaukhov, V. I. Kozlov, and O. P. Chervinko, "Analysis of stationary vibrations and dissipative heating of nonlinear viscoelastic bodies under periodic loading," *Prikl. Mekh*., **22**, No. 6, 49–55 (1986).
54. I. K. Senchenkov, V. G. Karnaukhov, V. I. Kozlov, and O. P. Chervinko, "A note on simple deformation in the vibration and heating problems for nonlinear viscoelastic bodies," *Prikl. Mekh*., **22**, No. 9, 82–90 (1986).
55. I. K. Senchenkov, V. G. Karnaukhov, and O. P. Chervinko, "The coefficient of energy absorption in cyclic deformation of viscoelastic materials and structural members," *Prikl. Mekh*., **24**, No. 9, 80–89 (1988).
56. I. K. Senchenkov, V. I. Kozlov, G. A. Tabieva, and V. A. Sanchenko, "Numerical simulation of the axisymmetric thermoviscoplastic state of solids of revolution under local thermal action," *Prikl. Mekh*., **33**, No. 2, 44–52 (1997).
57. I. K. Senchenkov and S. V. Novikov, "Spectral approach to the description of cyclic deformation and dissipative heating of viscoplastic bodies," *Prikl. Mekh*., **26**, No. 10, 76–84 (1990).
58. I. K. Senchenkov and G. A. Tabieva, "Determining the parameters of the Bodner–Partom model of thermoviscoplastic deformation," *Prikl. Mekh*., **32**, No. 2, 64–72 (1996).
59. I. K. Senchenkov, N. N. Yakimenko, and O. P. Chervinko, "Thermal fatigue failure of a rectangular prism with a cut. Numerical simulation and experiment," *Teor. Prikl. Mekh*., **39**, 42–47 (2004).
60. V. P. Tamusz and V. S. Kuksenko, *Fracture Micromechanics of Polymeric Materials* [in Russian], Zinatne, Riga (1978).
61. V. N. Poturaev (ed.), V. I. Dyrda, V. G. Karnaukhov et al., *Thermomechanics of Elastomer Structural Members under Cyclic Loading* [in Russian], Naukova Dumka, Kiev (1987).
62. C. Truesdell, *A First Course in Rational Continuum Mechanics*, The John Hopkins University, Baltimore (1972).
63. O. P. Chervinko, "Modeling vibrations in vibroprotection systems containing viscoplastic vibration isolators," *Mekh. Girosk. Sist*., **17**–**18**, 218–226 (2001–2002).
64. O. P. Chervinko, "Modeling vibrations in vibroprotection systems containing nonlinearly viscoelastic vibration isolators," *Mekh. Girosk. Sist*., **17–18**, 226–233 (2001–2002).
65. V. E. Shamanskii, *Numerical Methods for Solution of Boundary-Value Problems on an EDC-42 Computer* [in Russian], Naukova Dumka, Kiev (1966).
66. Ch. Adam and F. Ziegler, "Flexural vibrations of viscoplastic composite beam," in: *Proc. ICES-95*, July 30–August 3, Hawaii (1995).
67. Ch. Adam and F. Ziegler, "Moderately large forced oblique vibrations of elastic-viscoplastic deteriorating slightly curved beams," *Arch. Appl. Mech*., **67**, 375–392 (1997).
68. A. Benallal and D. Marquis, "Constitutive equations describing nonproportional effect in cyclic plasticity," in: *Constitutive Laws for Engineering Materials. Theory and Application*, Elsevier, New York (1987), pp. 505–572.
69. S. Bodner, *Unified Plasticity—an Engineering Approach* (Final Report), Faculty of Mechanical Engineering, Technion (Israel Institute of Technology), Haifa, Israel (2000).
70. S. R. Bodner and K. S. Chen, "Modelling of continuum damage for application in elastic-viscoplastic constitutive equations," *Eng. Fract. Mech*., **25**, No. 5/6, 705–712 (1986).
71. S. Bodner and A. Lindenfeld, "Constitutive modeling of stored energy of cold work under cyclic loading," *Eur. J. Mech., A/Solids*, **14**, No. 3, 333–348 (1995).
72. M. V. Borodii and V. A. Strizhalo, "Analysis of the experimental data on a low cyclic fatigue under nonproportional straining," *Int. J. Fatigue*, **22**, 275–282 (2000).
73. W. Brunner and H. Irschik, "An efficient algorithm for elasto-viscoplastic vibrations of multi-layered composite beams using second-order theory," *Nonlin. Dynam*., **1**, 1–12 (1994).
74. O. P. Chervinko and I. K. Senchenkov, "The coupled thermomechanical state of a notched viscoelastic rectangular plate under harmonic loading," *Int. Appl. Mech*., **38**, No. 2, 209–216 (2002).
75. L. J. Coffin, "Fatigue at high temperature—prediction and interpretation," in: *Proc. Inst. Mech. Eng*., **188**, No. 9, 109–127 (1974).
76. F. Ellyin, "A cyclic constitutive relations for multiaxial stress states," in: K.-T. Rie (ed.), *Proc. 2nd Int. Conf. on Low Cycle Fatigue and Elasto-plastic Behaviour of Materials*, 7–11 September, Munich (1987), pp. 165–170.
77. P. Fotiu, "Elastodynamics of thin plates with internal dissipative processes. Part I. Theoretical foundation," *Acta Mech*., **95**, 29–50 (1992).
78. P. Fotiu, H. Irschik, and F. Ziegler, "Analysis of viscoplastic sandwich beams using influence functions," *Mech. Struct. Mach*., **16**, 35–52 (1988).

79. P. Fotiu, H. Irschik, and F. Ziegler, “Modal analysis of elastic-plastic vibrations by integral equations,” *Eng. Anal. Bound. Elem*., **14**, 81–97 (1994).
80. D. R. Hayhurst, “Creep rupture under multi-axial state of stress,” *J. Mech. Phys. Solids*, **20**, 381–390 (1972).
81. H. Irschik, „Das Mohrsche Verfahren zur Berechnung von Biegebalken mit nichtlinearen Werkstoffgesetz,“ *Techn. Mech*., **6**, 21–28 (1985).
82. H. Irschik, “Biaxial dynamic bending of elstoplastic beam,” *Acta Mech*., **62**, 155–167 (1986).
83. H. Irschik and F. Ziegler, “Dynamic processes in structural thermoviscoplasticity,” *Appl. Mech. Review*, **48**, No. 6, 301–316 (1995).
84. Y. Jiang and P. Kurath, “Nonproportional cyclic deformation: critical experiments and analytical modeling,” *Int. J. Plasticity*, **13**, No. 8–9, 743–764 (1997).
85. E. Krempl and D. Yao, “The viscoplasticity theory based on overstress applied to ratchetting and cyclic hardening,” in: K.-T. Rie (ed.), *Proc. 2nd Int. Conf. on Low Cycle Fatigue and Elasto-plastic Behaviour of Materials*, 7-11 September, Munich (1987), pp. 137–148.
86. J. Lamaitre, *A Course on Damage Mechanics*, Springer-Verlag, Berlin (1992).
87. A. S. Nowick and B. S. Berry, *Anelastic Relaxation in Crystalline Solids*, Acad. Press, New York–London (1972).
88. A. R. Payne, “Hysteresis in rubber vulcanizates,” *J. Polym. Sci.: Polymer Symposia. Rubber and Rubber Elasticity*, No. 48, 169–196 (1974).
89. B. Poddar, F. C. Moon, and S. Mukherjee, “Chaotic motion of an elastic-plastic beam,” *J. Appl. Mech*., **55**, No. 1, 185–189 (1988).
90. I. K. Senchenkov and Y. A. Zhuk, “Thermomechanical coupling effects in the elastic-viscoplastic bodies with internal defect,” in: *Abstracts of* 20*th Int. Congr. on Theoretical and Applied Mechanics*, ICTAM, Chicago (USA) (2000), p. 225.
91. J. C. Snowdon, *Vibrations and Shock in Damped Mechanical Systems*, J. Willey, New York (1968).
92. P. S. Symonds and T. X. Yu, “Constitutive behavior in a problem of elastic-plastic beam dynamics,” *Trans. ASME*, *J. Appl. Mech*., **52**, 517–522 (1985).
93. E. Tanaka, S. Murakami, and M. Ooka, “Effects of plastic strain amplitudes on non-proportional cyclic plasticity,” *Acta Mech*., **57**, 559–575 (1985).
94. E. Tanaka and H. Okuchi, “Constitutive modeling of viscoplasticity incorporating non-proportional hardening effect,” *Trans. JSME*, *Ser. A*, **54**, 1588 (1988).
95. H. S. Tzou and L. A. Bergman, *Dynamics and Control of Distributed Systems*, Cambridge Univ. Press, Cambridge (1998).
96. Y. A. Zhuk and I. K. Senchenkov, “Study of the resonant vibrations and dissipative heating of thin-walled elements made of a physically nonlinear material,” *Int. Appl. Mech*., **38**, No. 4, 463–471 (2002).
97. Y. A. Zhuk and I. K. Senchenkov, “Approximate model of thermomechanically coupled inelastic strain cycling,” *Int. Appl. Mech*., **39**, No. 3, 300–306 (2003).
98. Y. A. Zhuk, O. P. Chervinko, and G. A. Tabieva, “Planar flexural vibration and dissipative heating of laminated rectangular plates,” *Int. Appl. Mech*., **38**, No. 7, 837–844 (2002).
99. Y. A. Zhuk, I. K. Senchenkov G. A. Tabieva, and O. P. Chervinko, “Axisymmetric vibrations and dissipative heating of a laminated inelastic disk,” *Int. Appl. Mech*., **38**, No. 1, 95–102 (2002).